

Carbon Kagome Nanotubes — quasi-one-dimensional nanostructures with flat bands

Hsuan Ming Yu^{a,**}, Shivam Sharma^{b,**}, Shivang Agarwal^c, Olivia Liebman^a, Amartya S. Banerjee^{a,*}

^a*Department of Materials Science and Engineering, University of California, Los Angeles, CA 90095, U.S.A*

^b*Department of Aerospace Engineering and Mechanics, University of Minnesota, Minneapolis, MN 55455, U.S.A*

^c*Department of Electrical and Computer Engineering, University of California, Los Angeles, CA 90095, U.S.A*

Abstract

In recent years, a number of bulk materials and heterostructures have been explored due their connections with exotic materials phenomena emanating from flat band physics and strong electronic correlation. The possibility of realizing such fascinating material properties in simple realistic nanostructures is particularly exciting, especially as the investigation of exotic states of electronic matter in wire-like geometries is relatively unexplored in the literature. Motivated by these considerations, we introduce in this work carbon Kagome nanotubes (CKNTs) — a new allotrope of carbon formed by rolling up Kagome graphene, and investigate this material using specialized first principles calculations. We identify two principal varieties of CKNTs — armchair and zigzag, and find both varieties to be stable at room temperature, based on ab initio molecular dynamics simulations. CKNTs are metallic and feature dispersionless states (i.e., *flat bands*) near the Fermi level throughout their Brillouin zone, along with an associated singular peak in the electronic density of states. We calculate the mechanical and electronic response of CKNTs to torsional and axial strains, and show that CKNTs appear to be more mechanically compliant than conventional carbon nanotubes (CNTs). Additionally, we find that the electronic properties of CKNTs undergo significant electronic transitions — with emergent partial flat bands and tilted Dirac points — when twisted. We develop a relatively simple tight-binding model that can explain many of these electronic features. We also discuss possible routes for the synthesis of CKNTs. Overall, CKNTs appear to be unique and striking examples of realistic elemental quasi-one-dimensional materials that may display fascinating material properties due to strong electronic correlation. Distorted CKNTs may provide an interesting nanomaterial platform where flat band physics and chirality induced anomalous transport effects may be studied together.

Abbreviations: CKNT - Carbon Kagome Nanotube, CNT - Carbon Nanotube, QBC - quadratic band crossing, TB - tight-binding, 1D - quasi-one-dimensional, 2D - quasi-two-dimensional.

Keywords: Carbon Kagome lattice, nanotube, flat band, strong correlation, strain engineering.

1. Introduction

Over the past two decades, the design, discovery and characterization of nanomaterials and nanostructures with special features in their electronic band structure has gained prominence. Exemplified famously by the case of linear dispersive relations in graphene (associated with massless Dirac fermions [1, 2]), such features often point to the existence of exotic electronic states, and the possibility of realizing unconventional electromagnetic, transport and optical properties in real systems. In recent years, materials and structures featuring dispersionless electronic states or *flat bands* have been heavily investigated due to the fact that electrons associated with such states have quenched kinetic energies¹ (are spatially localized), and interact in the strong correlation regime[3–6]. This manner of interaction leads to a variety of fascinating materials phenomena, including superconductivity [3, 7], ferromagnetism [8], Wigner crystallization [9, 10], and the fractional quantum Hall effect [11–14].

Along these lines, moiré superlattices in twisted bilayers [8, 15–19] and materials with tailored atomic lattices [20–23] have received much attention since they feature flat bands and rich electron physics. In order to observe and maintain desirable electronic properties, such systems usually involve some degree of engineering, and more often, a fine control over important system parameters (e.g. bilayer twists at specific *magic angles* [24], or a critical magnetic field strength in quasi-two-dimensional (2D) network structures [25, 26]). Therefore, a strand of recent investigations has focused on the synthesis and characterization of materials which feature electronic flat bands due to their natural atomic arrangements [27–35]. Exotic electronic states hosted by such materials can be stable with respect to perturbations such as changes in temperature or applied strains, and they can often display such states without external fields — features which make them suitable for device applications. Alongside these experimental studies, computational investigations have also probed elemental versions of such materials, i.e., stable bulk or 2D nanomaterials made of a single species of atom that can feature unusual electronic states by virtue of their atomic arrangements alone [36–39, 39–41]. The present study

*Corresponding author. Tel:+1-763-656-7830. E-mail: asbanerjee@ucla.edu

**Authors contributed equally

Email addresses: kingforever10@ucla.edu (Hsuan Ming Yu), sharm608@umn.edu (Shivam Sharma), shivangag97@ucla.edu (Shivang Agarwal), oliebman@ucla.edu (Olivia Liebman), asbanerjee@ucla.edu (Amartya S. Banerjee)

¹While linearly dispersive states are associated with extremely high charge carrier mobilities, flat band electrons are massive and effectively have zero group velocity.

extends this particular line of work to the important case of quasi-one-dimensional (1D) nanomaterials featuring flat bands, which have generally received far less attention in the literature.²

The possibility of realizing flat band physics and exotic states of electronic matter in wire-like geometries is particularly exciting. While well known theoretical considerations [45, 46] appear to preclude the existence of long range order in low dimensional systems (necessary, e.g. in realizing superconducting states), such restrictions do not necessarily apply to the quasi-one-dimensional structures considered here [47]. In fact, there are reasons to expect that the screw transformation symmetries and quantum confinement effects often associated with such systems can actually result in enhancement of collective or correlated electronic properties [48–50], and that such properties are likely to be manifested in manners that are quite different from bulk phase materials. In particular, materials such as the ones considered in this work can be *chiral* — due to intrinsic or applied twists — and therefore, feature anomalous transport (the Chiral Induced Spin Selectivity, or CISS effect [51, 52]). The exploration of simultaneous manifestations of such effects along with correlated electron physics has begun fairly recently [53–56]. We posit that the carbon nanostructures explored here are likely to emerge as a possible material platform for such studies in the future.

Due to its unique allotrope forming features and versatility [57–59], carbon is particularly attractive as a building block of novel materials. A large number of computational studies have recently been devoted to 2D and bulk allotropes of carbon displaying Dirac cones, flat bands and non-trivial topological states [37, 60–67]. On the other hand, although several 1D allotropes of carbon are well known [68–79], none of these systems are usually associated with flat band physics. As far as we can tell, there have been only a few earlier attempts at producing and investigating flat bands in realistic 1D nanomaterials of carbon: partially flat bands in zigzag graphene nanoribbons [80], spin polarized flat bands in hydrogenated carbon nanotubes [81], and moiré type flat bands in chiral carbon nanotubes with collapsed structures [82, 83] or incommensurate double wall geometries [84]. Our contribution aims to address this particular gap in the literature by studying a family of realistic 1D carbon nanostructures that naturally feature flat bands throughout their Brillouin zone. The flat bands in the structures presented here arise out of geometric and orbital frustration and without the aid of dopant or major structural instability effects, as employed in the aforementioned studies. Moreover, as we demonstrate, these dispersionless electronic states show fascinating transitions as the structures

²There has been recent work (see e.g. [6, 42–44]) on quasi-two-dimensional systems and heterostructures, featuring one-dimensional flat bands, or flat bands along specific directions of a two-dimensional Brillouin zone. In contrast, the systems studied here are all elemental quasi-one-dimensional (1D) nanostructures that feature flat bands throughout the entirety of their (one-dimensional) Brillouin zone.

are subjected to strains, while also proving to be robust and retaining many desirable characteristics in some respects.

To obtain a 1D carbon nanostructure with flat bands, our starting point is a planar sheet of Kagome graphene. We then “roll up” this 2D material along different directions to obtain Carbon Kagome Nanotubes (CKNTs). Kagome graphene and related bulk structures have recently received much attention in the materials literature [36, 38–41, 85, 86], and also in the physics literature, where the material is often identified as a “decorated honeycomb” or “star lattice” structure [23, 87–92]. Although Kagome graphene remains to be experimentally synthesized, successful synthesis of a variant of this material, i.e., nitrogen-doped graphene on a silver substrate — a 2D material with a Kagome pattern, has been carried out recently [93, 94]. Moreover, synthesis of novel complex nanotube structures in general (see e.g. [95]) and through the roll-up of 2D sheets in particular, is fairly common (see e.g. [96]), thus suggesting that CKNTs can be synthesized in the near future.

In this work, we introduce CKNTs, and carry out a thorough and systematic first principles characterization of this material in terms of its structural, mechanical and electromechanical properties. Wherever relevant, we provide comparisons of the properties of CKNTs against those of conventional carbon nanotubes (CNTs). All CKNTs studied here are metallic and feature flat bands (throughout their Brillouin zone) near the Fermi level, along with an associated singular peak in the electronic density of states. We show in particular that CKNTs appear to be more mechanically compliant when compared against CNTs, and that their electronic properties undergo significant electronic transitions — with emergent partial flat bands and Dirac points — when subjected to torsional strains. Our studies are made possible largely due to a suite of recently developed symmetry adapted electronic structure calculation techniques [97–103], that allow *ab initio* calculations of 1D materials and their deformed states to be carried out accurately and efficiently. We also develop a π -electron based tight binding model that includes up to next-nearest-neighbor interactions, which is able to capture many of the electronic properties of CKNTs, as revealed via first principles data.

The rest of the paper is organized as follows: Section 2 describes the geometry of the materials under study (subsection 2.1), as well as various aspects of the specialized first principles computational techniques used in this work (subsection 2.2). Section 3 presents results, touching on structural (subsection 3.1), mechanical (subsection 3.2), electronic (subsection 3.3.1) and electromechanical (subsection 3.3.2) aspects. We discuss possible routes to the synthesis of CKNTs in subsection 3.4 and conclude in Section 4. Details of the tight binding model for CKNTs are presented in Appendix Appendix A.

2. Material and Methods

In this section, we introduce the geometry of Carbon Kagome nanotubes (CKNTs) and their construction from Kagome graphene through the “roll up” procedure commonly employed in other similar types of nanomaterials [104, 105]. We also provide an outline of the various computational and theoretical methods used in our study.

2.1. From Kagome Graphene to Carbon Kagome Nanotubes

Several recent studies have explored the structure of Kagome graphene sheets and related bulk structures [23, 36, 38, 39, 41, 85]. As a starting point, we first consider the geometry of Kagome graphene. The hexagonal unit cell of this 2D material consists of 6 carbon atoms that form a pair of equilateral triangles, as shown in Fig. 1. We used

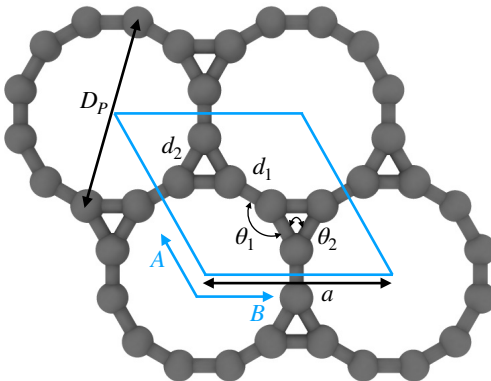


Figure 1: Unit cell of Kagome Graphene with various structural parameters indicated. The angle θ_1 is 150° , while θ_2 is 60° . The other parameters can be found in Table 1.

the planewave code ABINIT [106–108] to optimize the geometry of this structure. Our calculations employed norm conserving Troullier Martins pseudopotentials [109], an energy cutoff of 50 Ha, $21 \times 21 \times 1$ k-point sampling and Fermi-Dirac smearing of 0.001 Ha. These parameters were sufficient to produce accurate energies, forces and cell stresses for the pseudopotentials chosen [99]. We employed both Perdew-Wang [110] local density approximation (LDA) and Perdew-Burke-Ernzerhof (PBE)[111] generalized gradient approximation (GGA) exchange correlation functionals. At the end of the relaxation procedure, the atomic forces were typically of the order of 10^{-5} Ha/Bohr, while the cell stresses were of the order of 10^{-8} Ha/Bohr³.

Table 1 shows that the optimized structural parameters obtained by us are in very good agreement with the literature. As expected [112], the LDA bond lengths are somewhat shorter than those obtained through functionals involving gradient corrections, although the variations observed are quite minor overall. Notably, the intertriangle C-C

bond length was found to be slightly smaller than the bond length corresponding to the triangle sides. Additionally, the calculated bond angles were found to be 60° (in-triangle) and 150° (inter-triangle) almost perfectly, consistent with the literature. Next, following

| Parameters | Current work | Literature |
|------------|----------------------|------------------------------|
| a (Å) | $5.1370^a(5.1662)^b$ | $5.2085^c, 5.2087^d, 4.46^e$ |
| d_1 (Å) | $1.3402^a(1.3400)^b$ | $1.3559^c, 1.3567^d, 1.50^e$ |
| d_2 (Å) | $1.4078^a(1.4206)^b$ | $1.4305^c, 1.4299^d, 1.53^e$ |
| D_p (Å) | $5.3090^a(5.3331)^b$ | $5.3817^c, 5.3829^d$ |

Table 1: Optimized structural parameters of Kagome graphene. Superscripts denote parameters obtained using: (a) LDA functional (this work), (b) GGA functional (this work), (c) SGGA-PBE functional (reference [39]), (d) SGGA-PBE functional with Grimme D3 correction (reference [39]), and (e) GGA functional using the bulk structure (reference [40]).

the construction of carbon nanotubes from graphene [104, 113, 114], we rolled up the optimized flat Kagome graphene structures into seamless cylinders and arrived at carbon Kagome nanotubes (see Fig. 2). Depending on the direction of rolling, the tubes maybe armchair, zigzag or chiral, with non-negative integers (n, m) denoting the chirality indices. In this work, we focus exclusively on armchair (i.e., (n, n)) and zigzag (i.e., $(n, 0)$) nanotubes (illustrated in Fig. 3). The index n for such achiral tubes indicates the degree of cyclic symmetry about the tube axis. An investigation of chiral CKNTs is the scope of

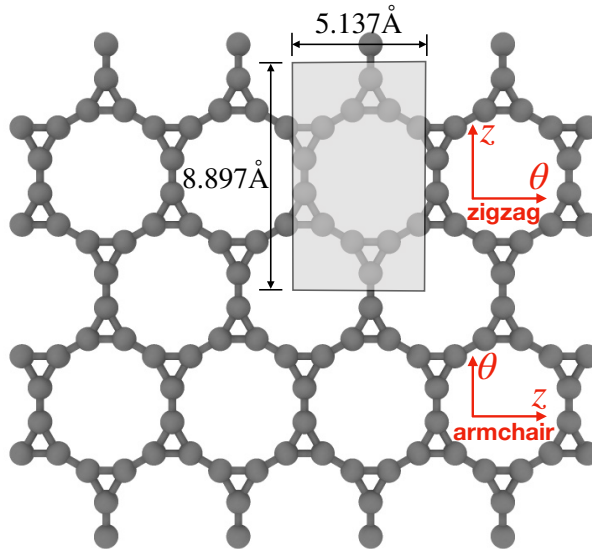


Figure 2: Roll-up construction of CKNTs, starting from a sheet of Kagome graphene. θ denotes the direction of roll up, while z denotes the tube axis direction. The 12 atoms shown in the shaded region are the representative atoms in the fundamental domain used for Helical DFT [98, 99] calculations. The domain size parameters illustrated above correspond to calculations based on LDA exchange-correlation.

future work. Notably, the replacement of hexagons in conventional CNTs, by dodecagonal rings in CKNTs, results in a structure with more porous sidewalls, and suggests the use of

this material in filtration [115], desalination [116] and electrochemical storage applications [117–119].

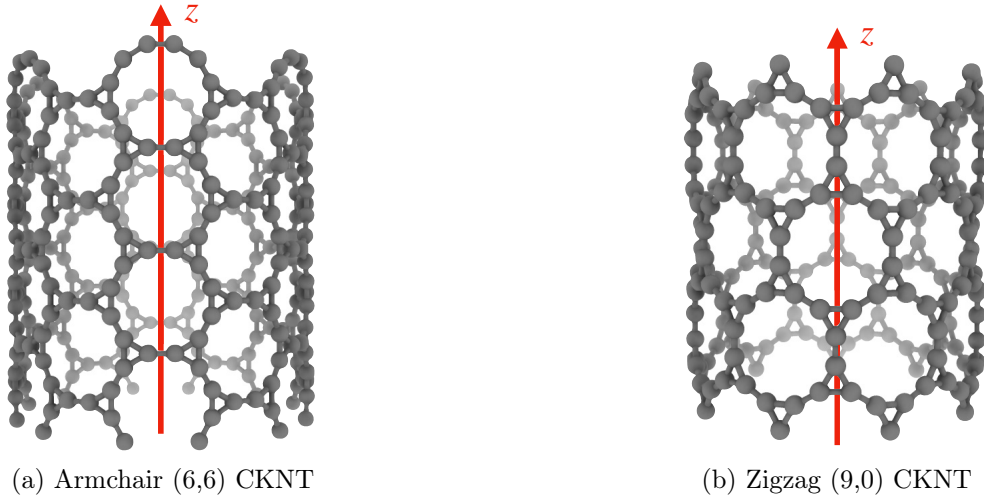


Figure 3: Two varieties of CKNTs investigated in this work: (a) Armchair (n, n) and (b) Zigzag $(n, 0)$ tubes. The tube radii are 0.85 nm and 0.74 nm, respectively for the above examples. n is the cyclic symmetry group order about the tube axis.

2.2. Computational Methods

We outline the computational methods employed in this work to study CKNTs. These include specialized, real-space symmetry adapted first principles simulations (using the Helical DFT code [98, 99]) and periodic plane-wave calculations (based on the ABINIT [106–108], Quantum Espresso [120–122] and PWDFT [123–126] codes), to augment the Helical DFT results. A tight-binding model which is able to replicate many of the electronic properties revealed by the above first principles calculations is detailed separately in Appendix A. In what follows, the atomic unit system with $m_e = 1$, $\hbar = 1$, $\frac{1}{4\pi\epsilon_0} = 1$ is used throughout, unless mentioned otherwise. We will denote the standard orthonormal basis of \mathbb{R}^3 with \mathbf{e}_x , \mathbf{e}_y , \mathbf{e}_z . Lowercase boldface letters will denote vectors in three dimensions, while uppercase boldface will denote matrices.

2.2.1. Helical DFT calculations

The majority of the first principles calculations in this work have been carried out using Helical DFT [98, 99] — a symmetry-adapted real-space formulation of Kohn-Sham Density Functional Theory [127]. We now highlight a few important features and technical details of this specialized computational technique. A key advantage of the methodology is its ability to efficiently simulate quasi-one-dimensional materials by exploiting global structural symmetries, which enables it to reduce calculations to just a few representative atoms within the simulation cell. The nanotubes of interest to this work, both in pristine

or deformed configurations, can be conveniently described using helical and cyclic symmetries about a common axis [49, 105, 128]. Specifically, for a nanotube with axis \mathbf{e}_z , if $\mathcal{P} = \{\mathbf{r}_1, \mathbf{r}_2, \dots, \mathbf{r}_M : \mathbf{r}_i \in \mathbb{R}^3\}$ are the coordinates of the representative atoms in the simulation cell (or *fundamental domain*), then the collection of coordinates of the entire structure can be expressed as:

$$\mathcal{S} = \bigcup_{\substack{\zeta \in \mathbb{Z} \\ \mu=0,1,\dots,\mathfrak{N}-1}} \bigcup_{i=1}^M \mathbf{R}_{(2\pi\zeta\alpha+\mu\Theta)} \mathbf{r}_i + \zeta\tau \mathbf{e}_z. \quad (1)$$

Thus, the symmetry group of the nanotube consists of the collection of isometries (i.e., rotations and translations):

$$\mathcal{G} = \left\{ \Upsilon_{\zeta,\mu} = (\mathbf{R}_{(2\pi\zeta\alpha+\mu\Theta)} | \zeta\tau \mathbf{e}_z) : \zeta \in \mathbb{Z}, \mu = 0, 1, \dots, \mathfrak{N} - 1 \right\}. \quad (2)$$

Here, each symmetry operation $\Upsilon_{\zeta,\mu}$ consists of a rotation operation about \mathbf{e}_z through the angle $2\pi\zeta\alpha + \mu\Theta$ (denoted via the action of the rotation matrix $\mathbf{R}_{(2\pi\zeta\alpha+\mu\Theta)}$ above), along with simultaneous translation by $\zeta\tau$ about the same axis. The quantity \mathfrak{N} is a natural number that captures cyclic symmetries in the nanotube, with the angle $\Theta = 2\pi/\mathfrak{N}$ (i.e., \mathfrak{N} is the same as n in armchair (n, n) and zigzag $(n, 0)$ nanotubes). The scalar α is related to the applied or intrinsic twist in the structure, with the amount of twist per unit length measured as $\beta = 2\pi\alpha/\tau$. The parameter τ is related to the pitch of screw transformation symmetries in the nanotube, and variations in this quantity enable extensions and compressions about the tube axis to be captured.

For the CKNTs considered in this work, we have employed an orthogonal unit cell with 12 representative atoms, as shown in Fig. 2. The parameter α takes values between 0 and 1, with $\alpha = 0$ representing untwisted structures. The value of τ as suggested by the roll-up construction [105, 129] is 5.137 Å and 8.897 Å for undeformed armchair and zigzag CKNTs, respectively.

Helical DFT uses a higher order finite difference discretization scheme in *helical coordinates* [97, 98] to solve the following symmetry adapted equations of Kohn-Sham DFT over the fundamental domain:

$$\mathfrak{H}^{\text{KS}} \psi_j(\mathbf{x}; \eta, \nu) = \lambda_j(\eta, \nu) \psi_j(\mathbf{x}; \eta, \nu). \quad (3)$$

The Kohn-Sham Hamiltonian operator:

$$\mathfrak{H}^{\text{KS}} = -\frac{1}{2}\Delta + V_{\text{xc}} + \Phi + \mathcal{V}_{\text{nl}}, \quad (4)$$

consists of kinetic energy, exchange correlation, electrostatic contribution (i.e., both electron-electron and electron-nucleus interactions) and non-local pseudopotential [130] terms. The symmetry-adapted quantum numbers $\eta \in [-\frac{1}{2}, \frac{1}{2})$, and $\nu \in \{0, 1, 2, \dots, \mathfrak{N}-1\}$ serve to label the eigenstates and electronic occupation numbers of the system (analogous to ‘k-points’ in periodic calculations of solids), along helical and cyclic symmetry directions, respectively. At the end of self-consistent solution of the above equations, the system’s ground state electronic free energy per unit fundamental domain may be calculated. We will denote this quantity as $\mathcal{F}_{\text{State}}^{\text{Ground}}(\mathcal{P}, \mathcal{D}, \mathcal{G})$ to signify its explicit dependence on the positions of the representative atoms within the fundamental domain (\mathcal{P}), the fundamental domain itself (\mathcal{D}), and the symmetry group of the structure under consideration (\mathcal{G}). By introducing variations in \mathcal{G} and by minimizing $\mathcal{F}_{\text{State}}^{\text{Ground}}(\mathcal{P}, \mathcal{D}, \mathcal{G})$ with respect to the coordinates of the representative atoms, Helical DFT can be employed for *ab initio* exploration of the deformation response of a nanomaterial under torsional or axial loads [99].

In order to facilitate the large number of ground state electronic structure calculations of various CKNTs as well as their electromechanical response under applied deformations, Helical DFT simulations were carried out in three stages. First, for a given nanotube and applied strain parameters, *ab initio* structural relaxation calculations were carried out using a mesh spacing of $h = 0.3$ Bohr, and by sampling 15 reciprocal space points in the η direction. These discretization choices are sufficient to produce chemically accurate forces and ground state energies for the norm conserving pseudopotential [130, 131] used to model the carbon atoms in this work [99]. Atomic relaxation was carried using the Fast Inertial Relaxation Engine [132] and calculations were continued until each atomic force component on every atom in the simulation cell reached 0.001 Ha/Bohr or lower. Next, for each relaxed structure, we redid a self-consistent calculation using the finest discretization parameters that could be reliably employed within computational resource constraints. This corresponds to a mesh spacing of $h = 0.25$ Bohr and 21 reciprocal space points in the η direction. This calculation step enables accurate calculations of energetics and stiffness parameters to be carried out [99]. Finally, using the self consistent densities and potentials obtained through the above step, we performed a single Hamiltonian diagonalization step using 45 reciprocal space points in the η direction. The eigenstates so obtained were used for band diagram and electronic density of states calculations that are presented in Section 3.

For all Helical DFT calculations, we used the Perdew-Wang parametrization [133] of the LDA[127]. We did not observe any major qualitative differences in the electronic properties between the LDA results presented here and those produced using gradient corrected functionals [111]. We also employed 12th order finite differences [98, 100, 134–139], vacuum padding of 10 Bohrs in the radial direction and 1 milli-Hartree of smearing

using the Fermi-Dirac distribution. The pseudopotential employed was generated using the Troullier-Martins scheme [109, 131], and is identical to the one used for the flat sheet calculations presented earlier (Section 2.1).

2.3. Plane-wave DFT calculations

We used plane-wave DFT [140, 141] for carrying out a few additional first principles calculations of CKNTs. Specifically, we investigated the dynamic stability of undistorted CKNTs by performing *ab initio* molecular dynamics (AIMD) simulations. The highly scalable PWDFFT code [123–126] was used for this purpose. We investigated two generic CKNTs — one each of the zigzag and armchair varieties — with radii of 0.75 and 0.85 nm for our simulations. In order to capture long range deformation modes, we considered atoms beyond the minimal periodic unit cell and chose multiple layers of the tubular structures along the axial direction. This resulted in supercells containing 144 and 216 atoms for the armchair and zigzag variety tubes respectively. Periodic boundary conditions were enforced along the axial direction and a large amount of vacuum padding (~ 35 Bohr) was included in the other two directions to prevent interactions between periodic images. Optimized Norm Conserving (ONCV) pseudopotentials [142, 143], and LDA exchange correlation were employed. An energy cutoff of 40 Ha was employed and only the gamma point of the Brillouin zone was sampled. The structures were first relaxed using the Broyden–Fletcher–Goldfarb–Shanno (BFGS) algorithm [144] following which AIMD simulations were performed at temperatures of 315.77 K, 631.55 K and 947.31 K using the Nosé–Hoover thermostat [145, 146]. Time steps of 1.0 fs were employed for integration and 5.0 – 7.0 ps of trajectory data were collected for analysis.

Finally, we used the Quantum Espresso code [120–122] for computing the projected density of states (PDOS) of undistorted armchair and zigzag CKNTs. Pseudopotentials from the Standard Solid State Pseudopotentials (SSSP) library [147, 148], along with an energy cutoff of 40 Ha, LDA exchange correlation and Gaussian smearing (corresponding to an electronic temperature of 315.77 K) were employed. Keeping in mind the geometry of the nanotube, the PDOS were calculated in the local atomic coordinate frame, i.e., the projections were taken on atomic orbitals that had been rotated to a basis in which the occupation matrix appears diagonal.

3. Results and Discussion

In this section, we discuss the structural, mechanical and electronic properties of CKNTs as revealed by our simulations.

3.1. Structural properties: Cohesive energy, sheet bending modulus and dynamic stability

Fig. 4 shows the cohesive energy of armchair and zigzag CKNTs as the tube radius varies in the range 1 to 3 nm (approximately). Owing to the contribution from the elastic

sheet bending energy, the cohesive energy of both types of tubes decrease monotonically as the tube radius increases, i.e., the tubes are energetically more favorable with decreasing sheet curvature. In our calculations, the energy of an atom in Kagome graphene, as calculated in terms of the large radius limit of the energies of CKNTs, agrees with direct calculations of the sheet to better than 1 milli-eV, thus ensuring overall consistency of the results. For a given radius, the zigzag and armchair CKNTs appear nearly identical energetically, similar to the behavior of conventional CNTs, also shown in Fig. 4. Assuming a quadratic dependence of the bending energy on curvature, i.e., Euler-Bernoulli behavior, we evaluated the area-normalized sheet bending modulus of Kagome graphene to be 0.506 eV and 0.502 eV in the armchair and zigzag directions, respectively (also see Fig. 2). This is about a third of the sheet bending modulus of conventional graphene, estimated to be about 1.5 eV through similar first principles calculations [100].

From Fig. 4, it is also evident that for a similar value of the radius, CNTs are energetically more favorable compared to CKNTs (i.e., CNTs have larger cohesive energies). We remark however that this observation in of itself does not preclude the synthesis of CKNTs. Indeed, fullerenes can be readily produced, although they have long been known to have cohesive energies that are somewhat lower than other common allotropes of carbon [104, 149–151]. More recently γ -graphyne, which has a significantly lower cohesive energy compared to graphene [152] has also been chemically synthesized [153–155]. Notably, there has also been success in synthesis of other unusual quasi-one-dimensional allotropes of carbon starting from conventional carbon nanotubes [73], which may be adopted for producing CKNTs.

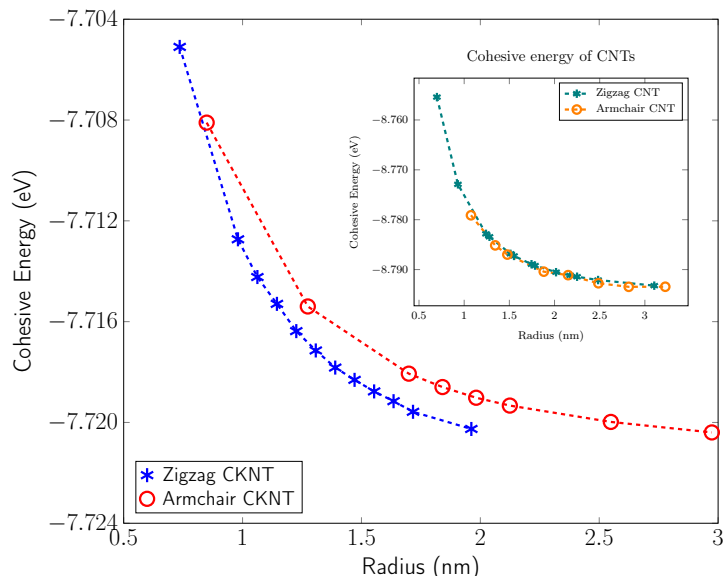


Figure 4: Cohesive energy of zigzag and armchair CKNTs. Inset: Cohesive energy of conventional zigzag and armchair carbon nanotubes (CNTs) presented for comparison.

The phonon stability of Kagome graphene sheets has been investigated earlier [41].

Based on band-folding considerations [156–158], such calculations are also likely to be indicative of the stability of CKNTs at zero temperature. To investigate the finite temperature structural stability of CKNTs, we carried out AIMD simulations at three different temperatures — 315.77 K, 631.54 K and 947.31 K. The system energy is observed to be stable throughout each of these simulations (Fig. 7). We conclude that CKNTs are able to maintain their overall structural integrity at room temperature, and beyond, thus making them physically realistic nanostructures. Notably, during the course of the simulations, the structures appear to undergo dynamic distortions similar to conventional CNTs [105, 159, 160], and show a propensity for developing transitory ellipsoidal cross sections, especially at elevated temperature (Fig. 6 (a)). Nevertheless, the dodecagonal rings which make up CKNTs and which are crucially related to their fascinating electronic properties (discussed in Section 3.3), continue to be maintained (Fig. 6 (b)). Given the relatively low sheet bending stiffness of Kagome graphene (as compared to conventional graphene, e.g.), it is quite possible that large diameter CKNTs, like their CNT counterparts [161–163] have a tendency to collapse. From this perspective, the distorted cross sections described above are possible indicators of this kind of structural transition, and warrant further investigation in the future. Snapshots of the AIMD simulations is provided in Figs. 5 and 6, and the entire simulation trajectories are available as Supplementary Materials.

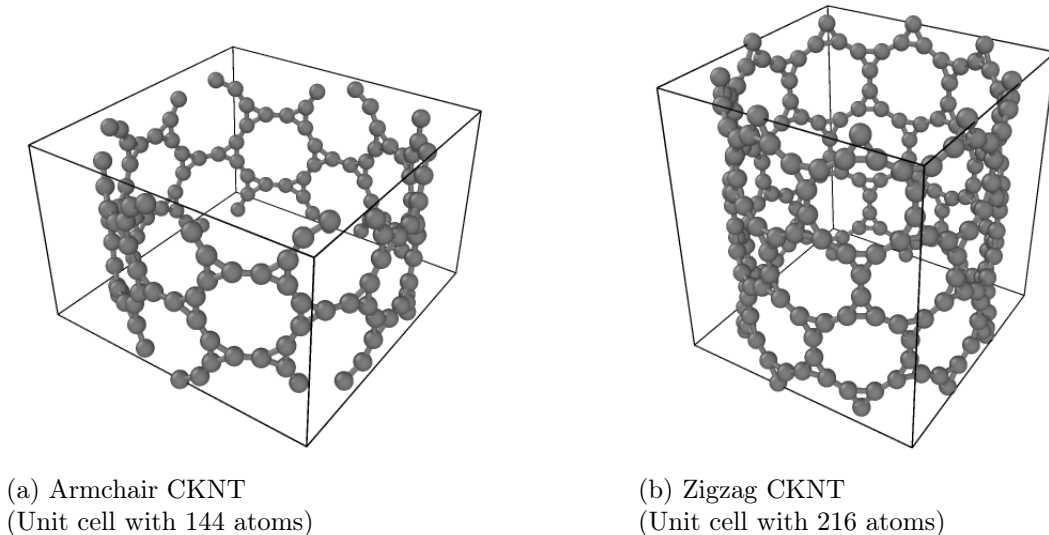


Figure 5: Snapshot of AIMD simulations at 315.77 K for both types of CKNTs.

3.2. Mechanical properties: Torsional and extensional stiffness

We focus on mechanical properties of CKNTs, namely their torsional and extensional responses in the linear elastic regime. As described earlier, Helical DFT allow such

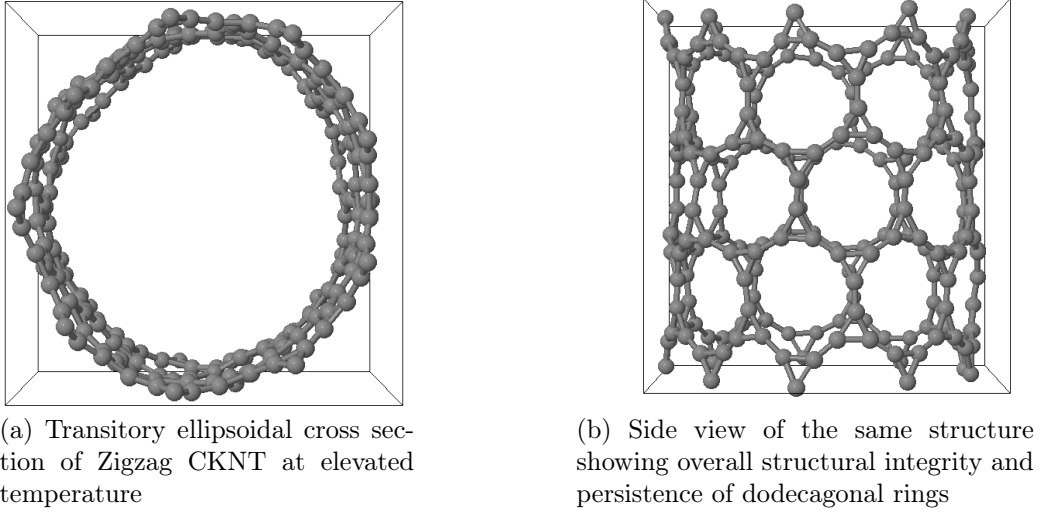


Figure 6: Snapshot of AIMD simulations of a Zigzag CKNT at an elevated temperature of 631.554 K. The cross-section shows a propensity for developing transitory distortions (left image). However, the overall structural integrity and the 12-fold rings continue to be maintained (right image).

calculations to be carried out by introducing changes in the nanotube symmetry group parameters. We consider (12, 12) armchair (radius 1.7 nm) and (12, 0) zigzag (radius 0.98 nm) CKNTs as representative examples. For both these tubes, we start from the undistorted, relaxed configurations.

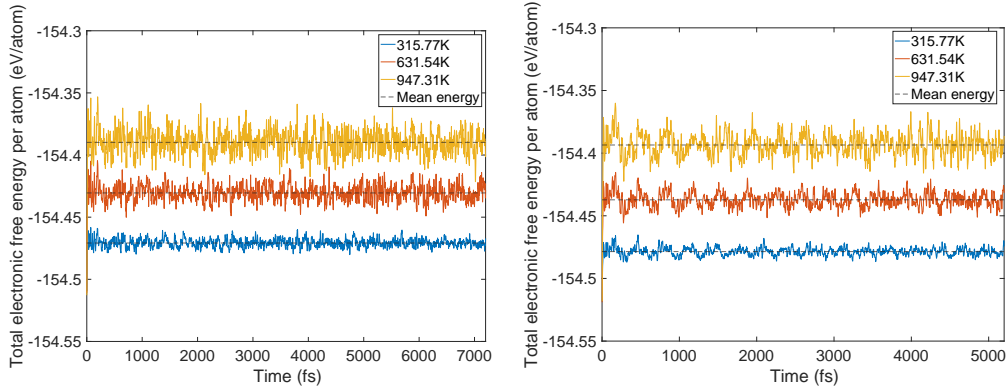
For simulations involving torsion, we increment the parameter α in regular intervals, imposing up to about $\beta = 4.5^\circ$ of twist per nanometer, the limit of linear response for conventional CNTs [105]. For each twisted configuration, we relax the atomic forces and compute the twisting energy per unit length of the nanotubes as the difference in the ground state free energy (per fundamental domain) of the twisted and untwisted structures, i.e.:

$$U_{\text{twist}}(\beta) = \frac{\mathfrak{N}}{\tau} \left(\mathcal{F}_{\text{Ground State}}(\mathcal{P}^{**}, \mathcal{D}, \mathcal{G}|_{\beta}) - \mathcal{F}_{\text{Ground State}}(\mathcal{P}^*, \mathcal{D}, \mathcal{G}|_{\beta=0}) \right). \quad (5)$$

In the equation above, $\mathcal{G}|_{\beta}$ and $\mathcal{G}|_{\beta=0}$ denote the symmetry groups associated with the twisted and untwisted structures, respectively and (as before) \mathfrak{N} denotes the cyclic group order. Additionally, \mathcal{P}^{**} and \mathcal{P}^* denote the collections of relaxed positions of the atoms in the fundamental domain in each case. Thereafter, the torsional stiffness is computed as:

$$k_{\text{twist}} = \left. \frac{\partial^2 U_{\text{twist}}(\beta)}{\partial \beta^2} \right|_{\beta=0}. \quad (6)$$

We observed that for the range of torsional deformations considered here, the behavior of $U_{\text{twist}}(\beta)$ is almost perfectly quadratic with respect to β , consistent with linear elastic



(a) Energy variation over ab-initio molecular dynamics trajectories over 7 ps of simulation time at 315.77 K (blue), 631.54 K (red) and 947.31 K (yellow) of an armchair CKNT. Black broken line represent the mean energy.

(b) Energy variation over ab-initio molecular dynamics trajectories over 5 ps of simulation time, at 315.77 K (blue), 631.54 K (red) and 947.31 K (yellow), of a zigzag CKNT. Black broken line represent the mean energy.

Figure 7: System energy variation over ab-initio molecular dynamics (AIMD) trajectories at three different temperatures for (a) an Armchair CKNT and (b) a Zigzag CKNT. The AIMD simulations reveal that the nanotubes maintains their overall structural integrity far above room temperature.

response (see Fig. 8). Moreover, the value of k_{twist} is estimated to be 3156.1 eV-nm and 979.51 eV-nm for the armchair and zigzag tubes, respectively. In the linear elastic regime, the torsional behavior of nanotubes is well approximated by continuum models which suggest that k_{twist} should vary with the tube radius in a cubic manner [99, 105, 164]. By use of this scaling law, we were able to estimate that conventional CNTs with radii comparable to the CKNTs considered above are expected to be significantly more rigid with respect to twisting (with k_{twist} values equal 2.8977×10^4 eV-nm and 5525.0 eV-nm for 1.7 nm and 0.98 nm radius conventional CNTs, respectively).

Next, for simulations involving axial stretch and compression, we proceed in a manner similar to the torsion simulations. For a given value of axial strain ϵ , we modify the pitch of the helical symmetry group as $\tau = \tau_0(1 + \epsilon)$, with τ_0 denoting the equilibrium, undistorted values. Subsequent to this kinematic prescription, we relax the atomic forces, and compute the extensional energy per unit length of the nanotubes as the difference in the ground state free energy per fundamental domain, between stretched and unstretched structures, i.e.:

$$U_{\text{stretch}}(\epsilon) = \frac{\mathfrak{N}}{\tau_0} \left(\mathcal{F}_{\text{State}}^{\text{Ground}}(\mathcal{P}^{**}, \mathcal{D}, \mathcal{G}|_{\tau=\tau_0(1+\epsilon)}) - \mathcal{F}_{\text{State}}^{\text{Ground}}(\mathcal{P}^*, \mathcal{D}, \mathcal{G}|_{\tau=\tau_0}) \right). \quad (7)$$

In the equation above, $\mathcal{G}|_{\tau=\tau_0(1+\epsilon)}$ and $\mathcal{G}|_{\tau=\tau_0}$ denote the symmetry groups associated with

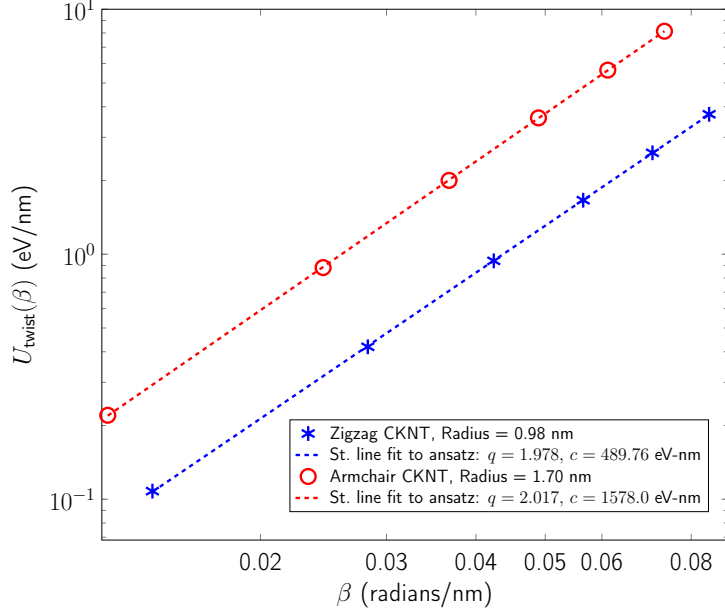


Figure 8: Twist energy per unit length as a function of angle of twist per unit length for two representative nanotubes (both axes logarithmic). Dotted lines indicate straight line fits of the data to an ansatz of the form $U_{\text{twist}}(\beta) = c \times \beta^q$. The exponent q is nearly 2 in both cases, suggesting linear elastic behavior.

the stretched and unstretched structures, respectively. Additionally, \mathcal{P}^{**} and \mathcal{P}^* denote the collections of relaxed positions of the atoms in the fundamental domain in each case. The stretching stiffness of the nanotubes may be then calculated as:

$$k_{\text{stretch}} = \left. \frac{\partial^2 U_{\text{stretch}}(\epsilon)}{\partial \epsilon^2} \right|_{\epsilon=0}. \quad (8)$$

In our simulations, we restricted ϵ to be between +3.6% and -3.6%. In this range, $U_{\text{stretched}}(\epsilon)$ is found to depend in a quadratic manner on ϵ , consistent with linear elastic behavior (see Fig. 9). We also observed a small Poisson effect, which we have ignored in subsequent analyses. For armchair (12, 12) and zigzag (12, 0) CKNTs, we estimated k_{stretch} to be 5220.9 eV/nm and 2093.4 eV/nm respectively. Based on scaling laws arising from continuum theory [164], we also estimated that conventional armchair CNTs with the same radii as the CKNTs considered above would be noticeably stiffer to axial deformations (k_{stretch} values equal to 1.2213×10^4 eV/nm and 7048.2 eV/nm for 1.7 nm and 0.98 nm radius conventional CNTs, respectively).

Overall, these results suggest that CKNTs are significantly more pliable with respect to torsional and axial deformations, as compared to their conventional CNT counterparts. Coupled with the lower bending stiffness of Kagome graphene as compared to conventional graphene, they are indicative of the fact that Kagome graphene has a lower value of in-plane (thickness normalized) Young's modulus and shear modulus.

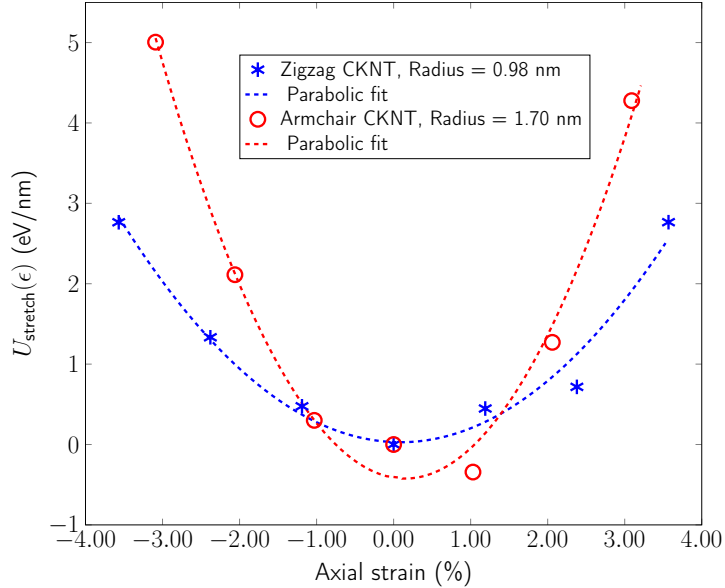


Figure 9: Extensional energy per unit length as a function of axial strain for two representative CKNTs. Dotted curves indicate parabolic fits of the data to an ansatz of the form $U_{\text{stretch}}(\epsilon) = c \times \epsilon^2$.

3.3. Electronic properties

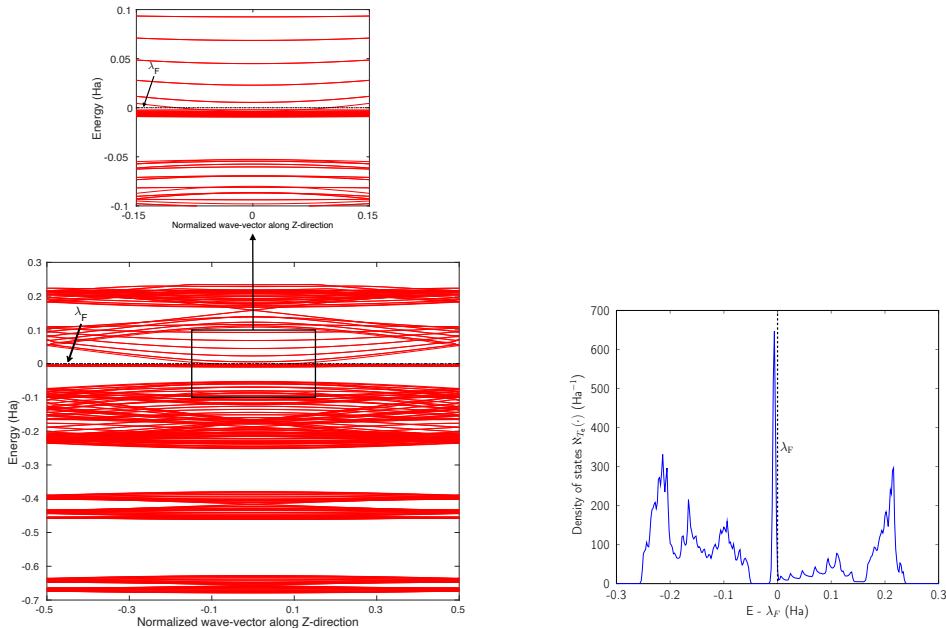
We discuss the electronic properties of CKNTs as revealed by first principles simulations. We start from a discussion of the properties of undistorted tubes, following which we discuss the electronic response of the tubes when subjected to torsional and axial strains. In [Appendix A](#) we describe a symmetry adapted tight-binding (TB) model that is able to explain these electronic properties.

3.3.1. Electronic properties of undeformed CKNTs

Conventional CNTs can be metallic or semiconducting depending on whether they are armchair (all tubes metallic) or zigzag (tubes with cyclic group order \mathfrak{N} divisible by 3 are metallic), and the electronic band diagrams of these materials prominently feature Dirac points near the Fermi level [99, 100, 104, 129, 165]. In contrast, our simulations reveal *all CKNTs* to be metallic, with their electronic band diagrams prominently featuring dispersionless electronic states, or *flat bands*, close to the Fermi level. Figs. 10a and 12a show complete band diagrams of undistorted CKNTs (i.e., all electronic states corresponding to allowable values of reciprocal space parameters η, ν are plotted), while Fig. 11 and 13 show symmetry adapted versions of these plots (i.e., band diagrams with chosen reciprocal space parameters along cyclic or helical directions). Notably, a CKNT of cyclic group order \mathfrak{N} is found to feature $2\mathfrak{N}$ nearly degenerate flat bands near the Fermi level. An associated singular peak in the electronic density of states (Figs. 10b, 12b) is also observed³, and both zigzag and armchair tubes are found to feature quadratic band crossing

³Our simulations suggest that the singular peak in the DOS of CKNTs occurs very close to the Fermi level — about 0.006 Ha away for the examples discussed here. In experimental situations, the peak in

(QBC) points at $\eta = 0$ (corresponding to the gamma point of the flat sheet). These features make CKNTs striking examples of realistic quasi-one-dimensional materials that are likely to exhibit strongly correlated electronic states. The detailed investigation of exotic materials phenomenon in CKNTs resulting from such strong electronic correlations — including e.g., Wigner crystallization, flat-band ferromagnetism and the emergence of superconducting, nematic or topological phases [41, 166, 167] — is the scope of future work. Considering that such phenomena have been studied primarily in bulk and two dimensional materials, the role that the quasi-one-dimensional morphology of CKNTs might play in them makes these investigations particularly interesting.



(a) Complete band diagram for an undistorted zigzag CKNT of radius 0.98 nm with a zoomed-in view of flat bands and quadratic band crossing point.

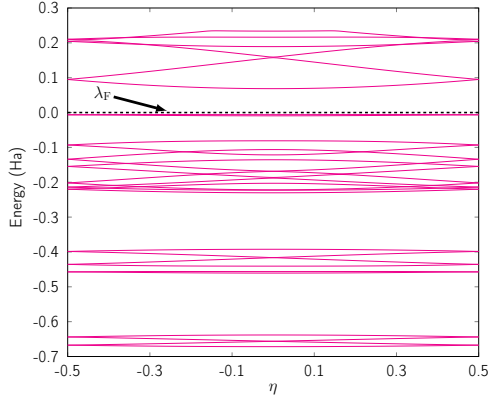
(b) Electronic density of states of the same material.

Figure 10: (a) Complete band diagram and (b) Electronic density of states near the Fermi level of an undistorted zigzag CKNT (radius 0.98 nm). λ_F denotes the Fermi level.

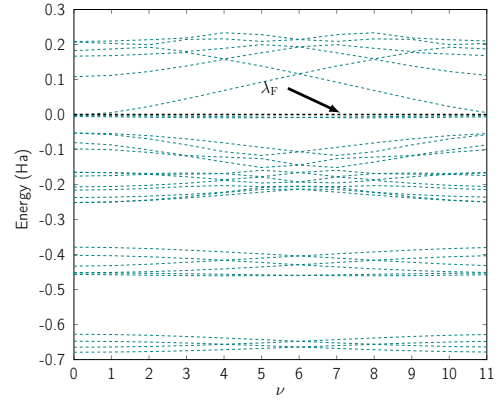
The dispersionless states in CKNTs are caused by destructive interference, resulting from geometric and orbital frustration, as has also been shown to occur in other Kagome lattice systems [168–170]. The electron effective mass is arbitrarily large at the flat band and the diminished electronic kinetic energy allows the Columbic interactions to dominate, resulting in strong electronic correlation. In turn, this causes electron localization⁴ and the emergence of a sharp peak (i.e., van Hove singularity [173]) in the electronic density of states (DOS) near the Fermi level (as shown in Figs. 10b and 12b). The localized

the DOS can be brought to the Fermi level exactly, by application of an external electric field or by doping [41], thus making the associated electronic states more readily accessible.

⁴The localization mechanism described above is different from Anderson localization, where electronic waves become diffusionless due to disorder/impurities in the system [171, 172].

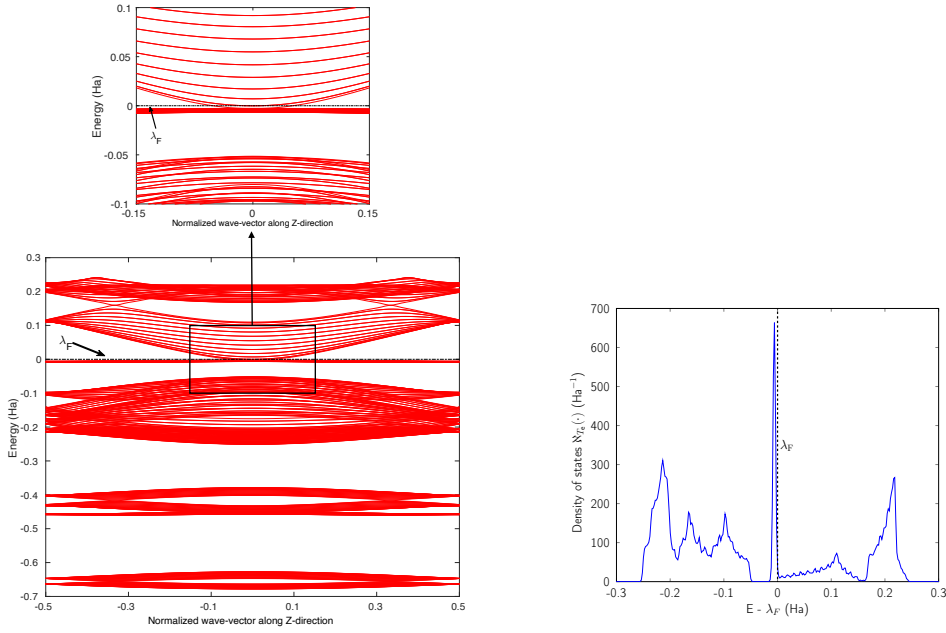


(a) Symmetry adapted band diagram in η , along $\nu = 4$.



(b) Symmetry adapted band diagram in ν , along $\eta = 0$. Quadratic band crossing at $\nu = 0$ can be observed.

Figure 11: Symmetry adapted band diagrams of an undistorted zigzag CKNT (radius 0.98 nm) obtained using Helical DFT [98, 99]. λ_F denotes the Fermi level.



(a) Complete band diagram for an undistorted armchair CKNT of radius 1.70 nm, with zoomed-in view of flat bands and quadratic band crossing point.

(b) Electronic density of states of the same material.

Figure 12: (a) Complete band diagram and (b) Electronic density of states near the Fermi level for the undistorted armchair CKNT (radius 1.70 nm). λ_F denotes the Fermi level.

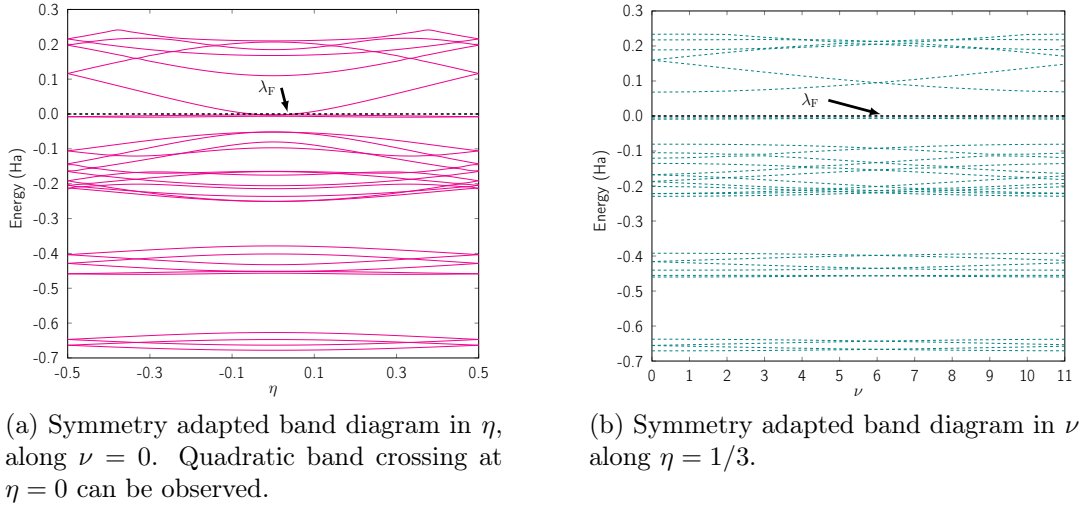


Figure 13: Symmetry adapted band diagrams of an undistorted armchair CKNT (radius 1.70 nm) obtained using Helical DFT [98, 99]. λ_F denotes the Fermi level.

states corresponding to an undistorted armchair CKNT are shown in Fig. 14a. A plot of the electron density distribution for that system is also shown (Fig. 14b).

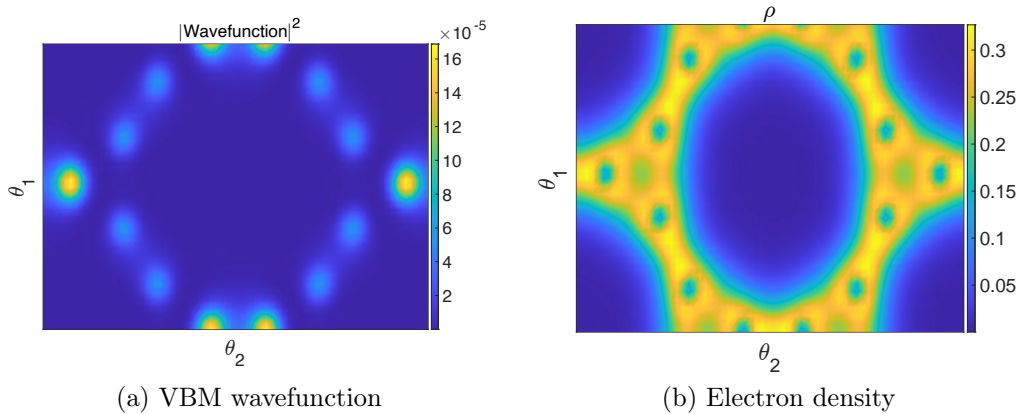


Figure 14: Valence Band Maximum (VBM) wavefunction and the electron density of an undeformed armchair (12, 12) CKNT. A slice of the electronic fields at the average radial coordinate of the atoms in the computational domain (represented using helical coordinates [98]) is shown.

At this point, it is worth mentioning some similarities of the electronic properties of CKNTs with their conventional counterparts. Like conventional CNTs, the fascinating electronic properties of CKNTs are largely connected to π electrons formed from radially oriented p_z orbitals, while the p_x and p_y orbitals form in-plane σ bonds and are largely electronically inactive [41]. This is supported by projected density of states (PDOS) calculations for CKNTs (Fig. 15), which show that the singular peak in the (total) electronic density of states near the Fermi level is largely attributable to the contributions of the individual (radially oriented) p_z ($l = 1, m_l = 0$) orbitals, while p_x and p_y orbital contributions lie well below the Fermi level. Moreover, the band diagrams of CKNTs have

some similarities in appearance with those of conventional CNTs, e.g., the presence of Dirac points at $\eta = 0$ for zigzag tubes and at $\eta = \pm\frac{1}{3}$ for armchair ones (Figs. 10a, 12a). However, unlike conventional CNTs, these Dirac points do not appear at the Fermi level in undistorted CKNTs, but are prominently featured as a part of the excited states of the system.

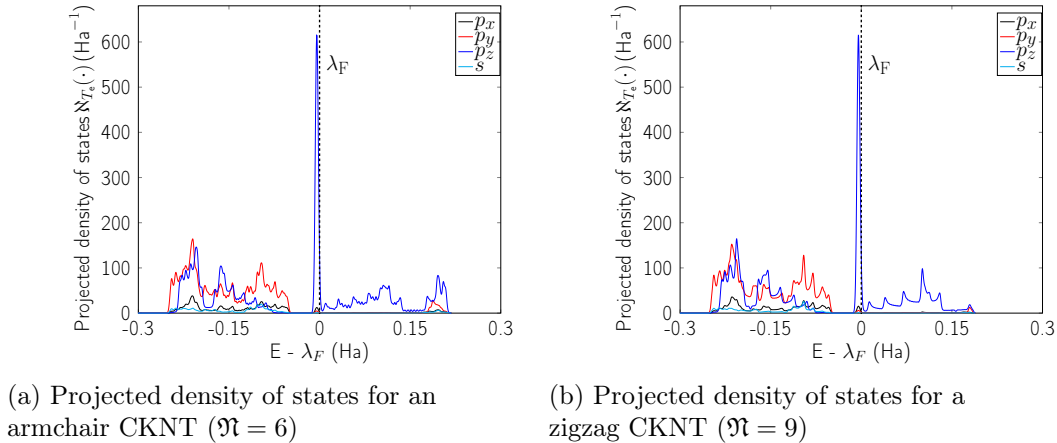


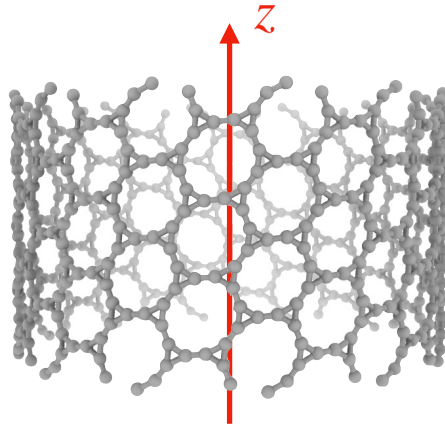
Figure 15: Projected density of states (PDOS) for undistorted armchair and zigzag CKNTs. The largest contribution to the sharp peak near the Fermi level is seen to arise from p_z orbitals.

3.3.2. Electromechanical response of CKNTs: Effect of torsional and axial strains on electronic properties

We discuss the changes to electronic properties of CKNTs to applied deformations. First, we discuss the effect of torsional strains. We use the (12, 12) armchair CKNT as a prototypical example; zigzag CKNTs are found to have similar behavior. As shown in Fig. 16a, application of twist to the CKNT destroys the in-plane C_6 symmetry of the underlying Kagome graphene lattice structure, while maintaining its C_2 symmetry. Consequently [174–176], the quadratic band crossing (QBC) point at $\eta = 0$ splits into a pair of Dirac points (Fig. 17a)⁵. Furthermore, the degeneracy in the $2\mathfrak{N}$ flat bands at the Fermi level appear to be lifted, and a number of dispersionless states appear to give way to bands that are only *partially flat*. The change of completely flat bands to ones which have some dispersion near $\eta = 0$ is also evidenced by the electronic density of states plot in Fig. 17b, which shows that the sharp peak near the Fermi level decays as the rate of applied twist increases. Despite these twist induced changes, a number of dispersionless states survive (Fig. 16a) and spatially localized wavefunctions associated with such states continue to be hosted by the nanotube (Fig. 16b). Notably, the application of twist results in energy dispersion relations that feature rather dramatic changes in the electronic

⁵The “tilted” nature of the linearly dispersive electronic bands near these Dirac points appears to suggest connections with (quasi-one-dimensional) Weyl semimetals [175, 177].

effective mass as the Brillouin zone is traversed — from infinitely massive carriers near $\eta = 0$, to massless ones as the Dirac points are reached, and then re-appearance of infinitely massive ones as the edge of the Brillouin zone is approached (i.e., closer to $\eta = \pm\frac{1}{2}$). Overall, these observations suggest that torsional strains provide a way of controlling correlated electronic states in CKNTs. Moreover, twisted CKNTs, being chiral, are likely to show asymmetric transport properties [51, 52]. Therefore, they provide an interesting, realistic material platform where the combined manifestations of anomalous transport phenomena (the Chiral Induced Spin Selectivity effect [178]) and flat band physics may be realized and studied.



(a) Armchair (12, 12) CKNT with $4.5^\circ/\text{nm}$ twist

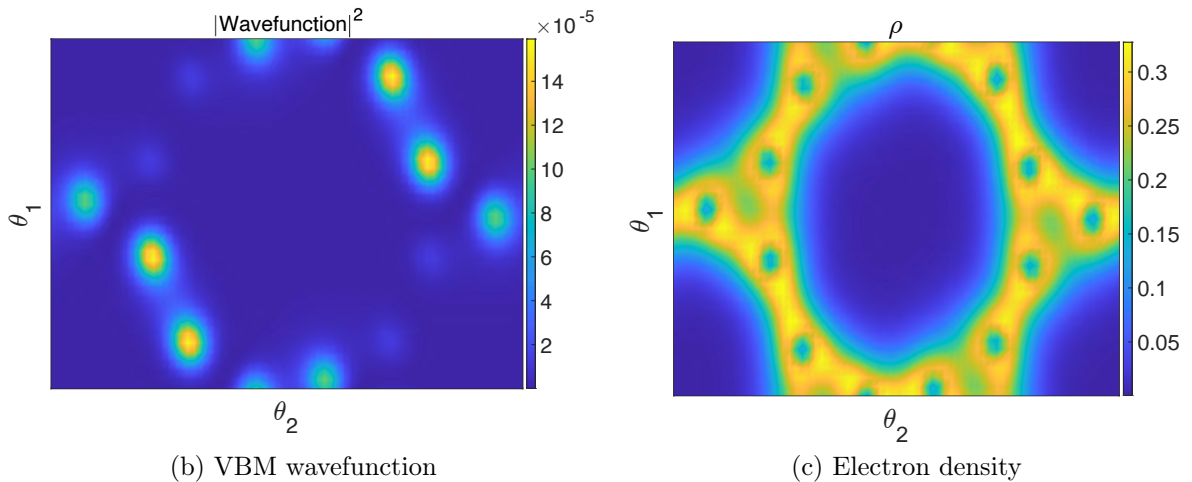
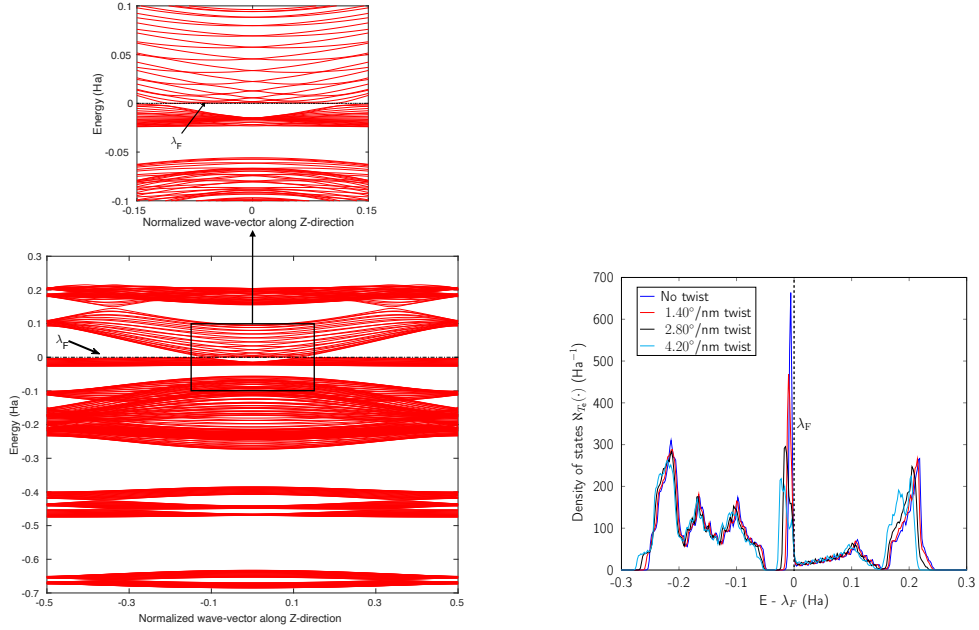


Figure 16: Atomic configuration, Valence Band Maximum (VBM) wavefunction and the electron density of an armchair (12, 12) CKNT with $\beta = 4.5^\circ/\text{nm}$ applied twist. A slice of the electronic fields at the average radial coordinate of the atoms in the computational domain (represented using helical coordinates [98]) is shown.

Next, we discuss the case of axial strains. In general, such deformations also tend to introduce some degree of dispersion into the flat bands of CKNTs near $\eta = 0$, while lifting their degeneracies near the Fermi level. However, their influence appears to be



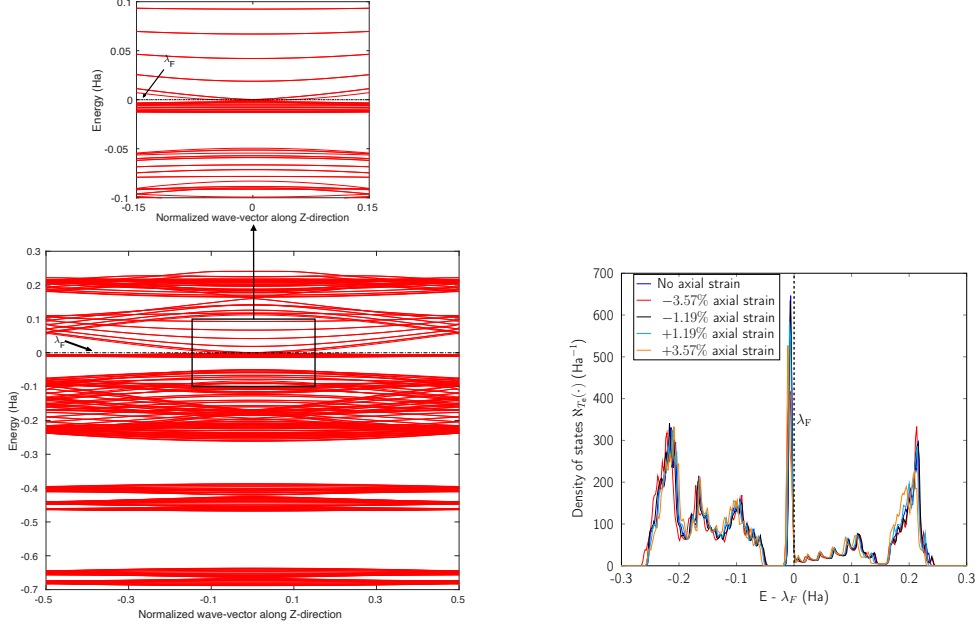
(a) Complete band diagram for a twisted armchair CKNT of radius 1.70 nm and a rate of twist of 4.20°/nm. Complete and partial flat bands, along with emergent Dirac points are featured. (b) Variation of the electronic density of states of the same material with twisting.

Figure 17: (a) Complete band diagram and (b) Electronic density of states near the Fermi level for the twisted armchair CKNT (radius 1.70 nm). λ_F denotes the Fermi level.

less dramatic than the case of torsional deformations described above. Nevertheless, the axial compression case deserves particular mention. Considering the zigzag (12,0) CKNT for example, we observe (see Fig. 18a) that the dispersion introduced in the flat bands near $\eta = 0$ results in curvature of these states in a manner that is opposite (i.e., convex vs. concave) of the situation encountered while twist is applied (i.e., Fig. 17a). Thus, a scenario akin to the touching of a pair of parabolic bands [176, 179] emerges. Upon subjecting the tube to larger values of compression, we observed that the parabolic bands near $\eta = 0$ give way to linear dispersion, i.e., the emergence of Dirac points. Commensurate with these changes, the sharp peak in electronic the density of states (Fig. 18b) also diminishes with increasing magnitude of axial strain, although the decrease appears to be less dramatic than the situation encountered with torsion (i.e., Fig. 17b).

Overall, the above observations are consistent with literature that suggests that quadratic band crossing points are unstable with respect to strains [180, 181]. It is also worthwhile at this point to contrast the electromechanical response of CKNTs to conventional CNTs. Zigzag CNTs with cyclic group order divisible by 3 and armchair CKNTs are both metallic [100], and they are known to be more sensitive to axial and torsional strains respectively. The effect of such deformations, at least for small strains, is to open up a gap at the Dirac points of these materials, resulting in metal-semiconductor

transitions [99, 165, 182–185]. As described above, CKNTs appear to show more dramatic electronic transitions when subjected to such strains. At the same time, the simulations above suggest that at least some dispersionless states in CKNTs are robust and continue to be available when the tube is subjected to small torsional and axial strains.



(a) Conventional band diagram for a stretched zigzag CKNT of radius 0.98 nm and an axial strain of -3.57% . (b) Variation in electronic density of states of the same material with applied axial strains.

Figure 18: (a) Complete band diagram and (b) Electronic density of states near the Fermi level for the stretched Zigzag CKNT (radius 0.98 nm). λ_F denotes the Fermi level.

3.3.3. Tight Binding Model

Based on the findings of the PDOS calculations (Fig. 15), we have developed a symmetry adapted tight binding (TB) model of the electronic structure of CKNTs. Our model involves π -electrons and incorporates up to next-nearest-neighbor interactions. The model is able to capture salient features of the electronic properties of undistorted CKNTs as revealed via first principles calculations. Additionally, by taking into account the variation in the hopping parameters with relative changes in bond lengths (eqs. A.5, A.7) the TB model is also able to account for the effects of strain on the electronic properties. We present details of the model in Appendix A. The TB model also produces results consistent with a π -orbital based empirical pseudopotential calculations [103, 186], but has the added advantage of being analytical in nature. Further analysis of the mathematical properties of the TB model is the scope of ongoing work [187].

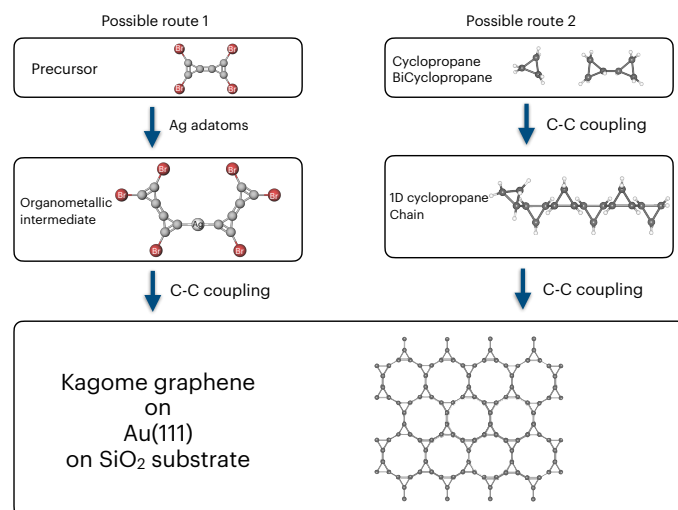
3.4. Possible routes to the synthesis of CKNTs

Our calculations suggest that CKNTs are kinetically stable, which is often taken to be a promising sign of the synthesizability of carbon allotropes [41, 188]. In the past, a wide variety of metastable carbon allotropes have been fabricated [189], often with significantly lower cohesive energies than other common stable counterparts. Examples of successful synthesis of such unusual carbon allotropes include γ -graphyne [152–155], T-carbon [73, 190] and nitrogen-doped Kagome graphene [93, 94]. In particular, various methods of synthesis of conventional carbon nanotubes, including laser ablation and chemical vapor deposition have been explored [191, 192]. Some of these techniques have also been successfully used in manufacturing other 1D carbon allotropes, e.g. T-carbon nanotubes, which can be created from conventional carbon nanotubes through a picosecond pulsed-laser irradiation induced first order phase transition. Such techniques provide additional routes for synthesizing CKNTs. Irrespective of the method, we anticipate that the analysis presented in this paper is likely to be instrumental in realizing CKNTs experimentally.

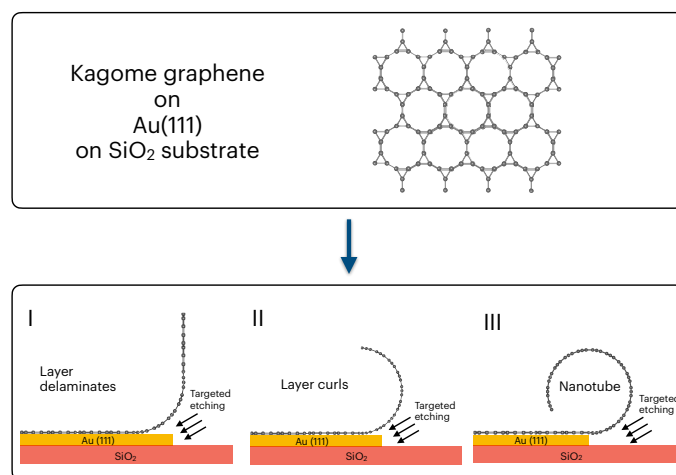
Since a variety of routes have been exploited for synthesizing different allotropes of carbon, multiple avenues also possibly exist for realizing CKNTs. We suggest two possibilities here, both based on the organic synthesis of Kagome graphene and subsequent roll-up of this material to form CKNTs. One possibility is to use silver adatoms to transform tetrabromobicyclopropane to intermediate organometallic complex and to then form Kagome graphene on the surface of SiO_2 substrate with etchant sensitive gold layer in between [93], as represented in left panel of Fig. 19a. The second possibility is through the use of cyclopropane or bicyclopropane [41, 188], wherein tailoring of ligand chemistry can be used to form self-assembled kagome graphene on the surface of gold (111), deposited on a SiO_2 substrate (shown in right panel of Fig. 19a). This latter method is similar to recently demonstrated self-assembly procedures in metastable carbon nanowigglers [193, 194]. After the synthesis of Kagome graphene, targeted etching of the gold layer [195] can result in the curling of the 2D material into CKNTs, as desired. The lower bending stiffness of kagome graphene in contrast to conventional graphene (Section 3.1) will likely assist in this step (Fig.19b).

4. Conclusion

In summary, we have introduced carbon Kagome nanotubes (CKNTs) — a new allotrope of carbon formed through a roll-up construction of Kagome graphene. These nanotubes are unique in the sense that contemporarily, they are perhaps the only known example of realistic, elemental, 1D nanostructures that can host dispersionless electronic states, or *flat bands*, in the entirety of their (one-dimensional) Brillouin zone. They also feature Dirac points in their band diagram, as well as a singular peak in their electronic



(a) Two possible ways to fabricate 2D flat sheet of Kagome graphene. Left panel: From tetrabromobicyclopropene to organometallic intermediate with Ag adatoms to the formation of final 2D sheet of carbon kagome lattice on Au(111) etchant material on SiO₂ substrate. Right Panel: From cyclopropane or bicyclopropane to 1D chain of cyclopropane to 2D sheet of carbon kagome lattice on Au(111) etchant material on SiO₂ substrate.



(b) Formation of Carbon kagome nanotube from Kagome graphene. After the target etching of Kagome graphene layer on Au etchant sensitive material on SiO₂ substrate surface the layer is curled up on to the sample surface where it can form bonds with itself.

Figure 19: Possible routes of synthesis of CKNTs. (a) Two possible routes to synthesis Kagome graphene. (b) Rolling up of a layer of Kagome graphene by target itching to form CKNTs.

density of states. Thus, they provide an attractive platform for studying and exploiting strongly correlated electronic phenomena in nanomaterials with wire-like geometries.

To characterize CKNTs, we have carried out an extensive series of first principles simulations, including specialized calculations based on symmetry adaptation. We have investigated both zigzag and armchair varieties of CKNTs. Cohesive energy computations and ab initio molecular dynamics simulations suggest CKNTs should exist as stable structures at room temperature and beyond. Our simulations reveal that it is easier to roll Kagome graphene into CKNTs than it is to roll conventional graphene into CNTs. Moreover, CKNTs are found to be significantly more pliable with respect to torsional and extensional deformation as compared to CNTs of similar radii. Both zigzag and armchair varieties of CKNTs are found to be metallic, and are seen to feature multiple degenerate flat bands and a corresponding singular peak in the electronic density of states, near the Fermi level. We studied the response of electronic properties of CKNTs to applied torsional and axial strains and showed that such deformations are very effective in inducing large changes in the electronic states of this material. We also developed a tight binding model which is able to capture many of the electronic properties of CKNTs observed in first principles calculations, and also reproduces correctly, the effect of strains in the material.

Given the relative stability of CKNTs and the fact that there has been recent successes in experimentally synthesizing various novel carbon allotropes, it appears likely that CKNTs can be produced and studied under laboratory conditions in the near future. Such pursuits, as well as more detailed characterizations of electronic phenomena in CKNTs at a level beyond Density Functional Theory, and the exploration of anomalous transport phenomena in distorted CKNTs, are all attractive directions of future research.

—

Appendix A. Tight binding model for CKNTs

We have developed a p_π -orbital based tight-binding (TB) model for understanding the electronic structure of CKNTs. As described below, to correctly reproduce the findings of the ab initio calculations, especially the effects of strain, we found it necessary to include up to next-nearest-neighbor (NNN) interactions and to make the hopping amplitudes dependent on relative changes in bond lengths. The TB Hamiltonian in second quantization framework [196, 197] is written as:

$$\begin{aligned} \mathbf{H} = & \sum_{i,\gamma} \varepsilon_{i\gamma} \mathbf{a}_{i\gamma}^\dagger \mathbf{a}_{i\gamma} + \sum_{\gamma} \sum_{\langle i,j \rangle} t_{1(i\gamma,j\gamma)} \mathbf{a}_{i\gamma}^\dagger \mathbf{a}_{j\gamma} \\ & + \sum_{\gamma} \sum_{\langle\langle i,j \rangle\rangle} t_{2(i\gamma,j\gamma)} \mathbf{a}_{i\gamma}^\dagger \mathbf{a}_{j\gamma} + \text{h.c.} . \end{aligned} \quad (\text{A.1})$$

Here, $\varepsilon_{i\gamma}$ denotes the onsite energy of site i and orbital γ , $t_{1(i\gamma,j\gamma)}$ and $t_{2(i\gamma,j\gamma)}$ are the hopping amplitudes between orbitals γ of the nearest-neighbors (NNs) $\langle i, j \rangle$ and the next-nearest-neighbors (NNNs) $\langle\langle i, j \rangle\rangle$, respectively, and h.c. is the hermitian conjugate. The annihilation and creation operators are denoted by $\mathbf{a}_{i\gamma}$, $\mathbf{a}_{i\gamma}^\dagger$, respectively. The onsite energy, $\varepsilon_{i\gamma}$, is considered zero for convenience. To calculate the TB band structure of CKNTs, we adopt the Dresselhaus method [104]. This procedure involves development of a TB formulation for the flat sheet (i.e., Kagome graphene), and subsequent mapping of the atoms of the two-dimensional lattice to a cylinder, so as to invoke boundary conditions appropriate to the nanotube. Details of these steps are discussed below.

Results from our TB calculations are presented in Figs. A.20 and A.21. As can be seen, there is excellent qualitative agreement between these results and the first principles data presented earlier.

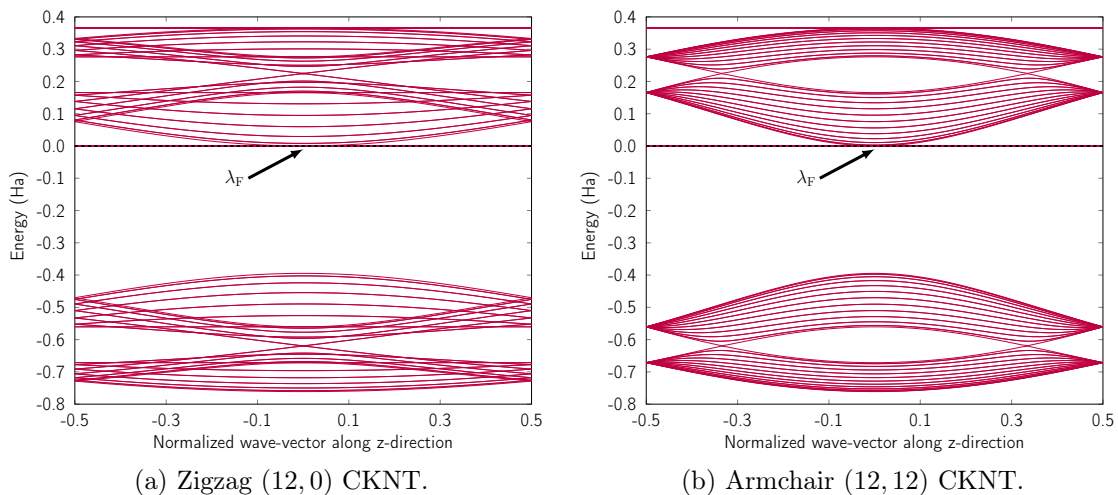


Figure A.20: Band diagram of undistorted CKNTs obtained from the tight binding model: (a) Armchair and (b) Zigzag cases shown. λ_F denotes the Fermi level.

Appendix A.1. Tight Binding model for Kagome graphene

The hexagonal unit cell of Kagome Graphene consist of two triangular sublattices A and B (Fig. A.22), consisting of a total of six Carbon atoms per unit cell. We consider only p_z orbitals in the TB method which yield a 6×6 TB hamiltonian, written in momentum space for NN interactions as [41]:

$$\mathbf{H}_{\text{Kagome Graphene}}^{\text{NN}} = \begin{pmatrix} \mathbf{H}_{AA} & \mathbf{H}_{AB} \\ \mathbf{H}_{BA} & \mathbf{H}_{BB} \end{pmatrix}, \quad (\text{A.2})$$

Axial or torsional strains in CKNTs can be mapped to appropriate deformations in Kagome graphene. For example, torsional strains in CKNTs have the effect of inducing a shear strain in the underlying Kagome graphene lattice. Generally, such distortions

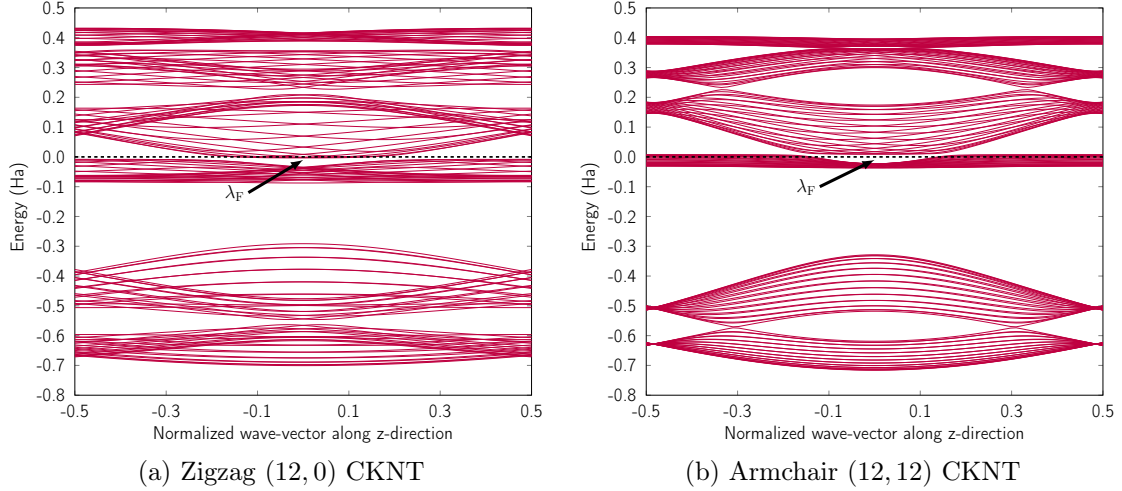


Figure A.21: Band diagram of twisted CKNTs obtained from the tight binding method, with about $4.8^\circ/\text{nm}$ of applied twist. λ_F denotes the Fermi level.

transform the sublattices in Kagome graphene from being perfect equilateral triangles to scalene triangles, so that the hopping matrix of sublattice B will no longer be the hermitian conjugate of that of sublattice A . The NN hopping matrix \mathbf{H}_{AA} of the sublattice A can be written as (refer to Fig. A.22):

$$\mathbf{H}_{AA} = \begin{pmatrix} 0 & t_{1ab}e^{ix_{2ab}\mathbf{a}_1\cdot\mathbf{k}} & t_{1ac}e^{ix_{2ac}\mathbf{a}_2\cdot\mathbf{k}} \\ t_{1ab}e^{-ix_{2ab}\mathbf{a}_1\cdot\mathbf{k}} & 0 & t_{1bc}e^{ix_{2bc}\mathbf{a}_3\cdot\mathbf{k}} \\ t_{1ac}e^{-ix_{2ac}\mathbf{a}_2\cdot\mathbf{k}} & t_{1bc}e^{-ix_{2bc}\mathbf{a}_3\cdot\mathbf{k}} & 0 \end{pmatrix}, \quad (\text{A.3})$$

while the inter-triangular hopping matrix \mathbf{H}_{AB} can be written as:

$$\mathbf{H}_{AB} = \text{Diag}[t'_{1ae}e^{ix_{1ae}(\mathbf{a}_1+\mathbf{a}_2)\cdot\mathbf{k}}, t'_{1cd}e^{-ix_{1cd}(\mathbf{a}_2-\mathbf{a}_3)\cdot\mathbf{k}}, t'_{1bf}e^{-ix_{1bf}(\mathbf{a}_1+\mathbf{a}_3)\cdot\mathbf{k}}], \quad (\text{A.4})$$

The matrices \mathbf{H}_{BB} and \mathbf{H}_{BA} can be written in the similar manner, and are not shown here for brevity. Consistent with the geometry of Kagome graphene and the mapping of strains from CKNTs to the Kagome graphene lattice, we choose $\mathbf{a}_1 = [1, 0, 0]$, $\mathbf{a}_2 = [\cos(\theta_0 + 2\pi\alpha), \sin(\theta_0 + 2\pi\alpha), 0]$ and $\mathbf{a}_3 = \mathbf{a}_1 - \mathbf{a}_2$ as the unit vectors in real space, and we further set $\theta_0 = \frac{\pi}{3}$. We denote $\mathbf{k} = [k_x, k_y]$ as the unit vector in reciprocal space.

The hopping amplitudes depend on the structure of the lattice and the applied deformations, and can be written as the function of relative change in bond length [198]:

$$\begin{aligned} t_{1uv} &= t_1^o \left(\exp\left(\frac{x_2 - x_{2uv}}{x_2}\right) \right)^n \quad \text{and} \\ t'_{1uv} &= t_1^{\prime o} \left(\exp\left(\frac{x_1 - x_{1uv}}{x_1}\right) \right)^n. \end{aligned} \quad (\text{A.5})$$

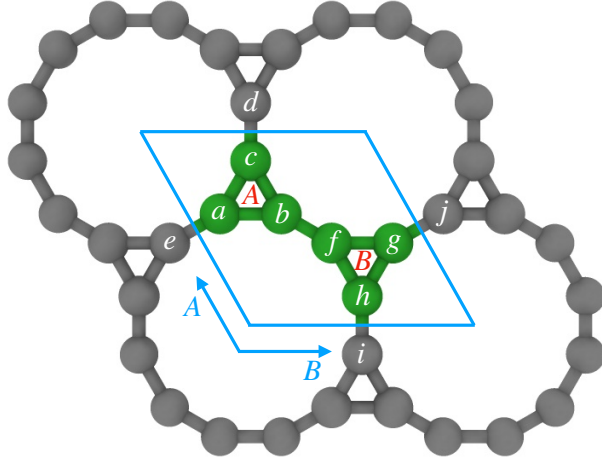


Figure A.22: Kagome Graphene structure with two sublattices A and B consisting of total six carbon atoms in the unit cell.

Here $t_1^0 = -5$ eV, $t_1^o = -7$ eV are the NN hopping parameters [199], and x_1 and x_2 are inter- and intra-triangular bond lengths in the undeformed structure (Fig. 1). The bond lengths x_{2uv} and x_{1uv} are in the deformed system, and u, v run over the NN atoms as shown in Fig. A.22. The parameter n controls the magnitude of the hopping parameter upon deformation of the lattice and parameterizes the “flatness” of the dispersionless states. Here, α is the nanotube’s applied twist parameter, as explained earlier in section 2.2.1. Following literature [198], we use $n = 8$ for getting both relatively flat bands and smooth evolution of band structure upon deformation.

The NNN interactions in our TB Hamiltonian take the following form:

$$\mathbf{H}_{\text{Kagome Graphene}}^{\text{NNN}} = \begin{pmatrix} \mathbf{0} & \mathbf{H}_{\text{NNN}} \\ \mathbf{H}_{\text{NNN}}^\dagger & \mathbf{0} \end{pmatrix}, \quad (\text{A.6})$$

here, hopping matrix $\mathbf{H}_{\text{NNN}}(u, u) = 0$ and $\mathbf{H}_{\text{NNN}}(u, v) = t_{2uv} e^{i\mathbf{k} \cdot \mathbf{x}_{3uv}}$, for $u \neq v$. The NNN hopping parameter is given as:

$$t_{2uv} = t_2^o \left(\exp \left(\frac{x_3 - x_{3uv}}{x_3} \right) \right)^n. \quad (\text{A.7})$$

Here x_3 is the distance between the NNN in the original structure and x_{3uv} is the same distance in the deformed nanotube; u, v denote the NNN atoms; and $t_2^o = -0.0125$ eV.

Appendix A.2. (n, m) nanotube and boundary conditions

To adapt the TB model of Kagome graphene described above to CKNTs, we follow the method developed by Dresselhaus [104]. The general procedure starts by considering

a semi-infinite two-dimensional sheet, whereby the two opposite edge sides are glued together to form an infinite tube, with the axis of the tube chosen to be the \mathbf{e}_z -direction. The periodicity along the circumferential direction naturally imposes periodic boundary conditions on the circumferential wave vector, denoted \mathbf{k}_\perp below. In what follows, we briefly describe the procedure for imposing such periodic boundary conditions on a nanotube constructed from an arbitrary two-dimensional lattice. Axial and torsional deformations in the nanotube can be naturally incorporated by considering the effect of applied strains to the two-dimensional lattice.

We first describe the construction of an (n, m) nanotube by rolling up a flat sheet along the direction of a *chiral vector*. The flat sheet is assumed to be generated using a 2D hexagonal lattice, with lattice vectors \mathbf{a}_1 and \mathbf{a}_2 , each of length a_0 (the lattice vectors for Kagome graphene are given in [Appendix A.1](#) above). The chiral vector for a nanotube with chirality (n, m) is then $\mathbf{C}_h = n\mathbf{a}_1 + m\mathbf{a}_2$, where n, m are non-negative integers. The *translation vector* which is parallel to the axis of the nanotube is expressed as $\mathbf{T} = T_1\mathbf{a}_1 + T_2\mathbf{a}_2$. Furthermore, $\gcd(T_1, T_2) = 1$, $T_1, T_2 \in \mathbb{Z}$, and:

$$T_1 = \frac{2m + n}{d_r}, T_2 = -\frac{2n + m}{d_r}, d_r = \gcd(2m + n, 2n + m).$$

The translation vector determines the axial periodicity of the nanotube, such that in real space, the unit cell of the nanotube is described by a rectangle generated by $\mathbf{C}_h \times \mathbf{T}$. The reciprocal lattice vectors corresponding to \mathbf{C}_h and \mathbf{T} are \mathbf{k}_\perp and \mathbf{k}_\parallel , respectively. Since, \mathbf{C}_h and \mathbf{T}_h are orthogonal vectors, this gives $\mathbf{C}_h \cdot \mathbf{k}_\perp = 2\pi$, $\mathbf{C}_h \cdot \mathbf{k}_\parallel = 0$, $\mathbf{T} \cdot \mathbf{k}_\perp = 0$, and $\mathbf{T} \cdot \mathbf{k}_\parallel = 2\pi$. By substituting \mathbf{k}_\perp and \mathbf{k}_\parallel into the orthogonality constraints, we get:

$$\mathbf{k}_\perp = \frac{1}{\mathcal{N}}(-T_2\mathbf{b}_1 + T_1\mathbf{b}_2), \quad (\text{A.8})$$

$$\mathbf{k}_\parallel = \frac{1}{\mathcal{N}}(m\mathbf{b}_1 - n\mathbf{b}_2), \quad (\text{A.9})$$

where, $\mathbf{b}_1 = \frac{2\pi}{a_0}(\mathbf{a}_2 \times \mathbf{z})$ and $\mathbf{b}_2 = \frac{2\pi}{a_0}(\mathbf{z} \times \mathbf{a}_1)$ are the unit vectors of the reciprocal lattice of the two-dimensional lattice, a_0 is the lattice parameter, and \mathbf{z} is perpendicular to both \mathbf{a}_1 and \mathbf{a}_2 . Furthermore, \mathcal{N} is the number of primitive unit cells per nanotube unit cell, and can be expressed as:

$$\mathcal{N} = \frac{|\mathbf{C}_h \times \mathbf{T}|}{|\mathbf{a}_1 \times \mathbf{a}_2|}. \quad (\text{A.10})$$

Note that, for the zigzag and armchair tubes considered here, \mathcal{N} is related to the cyclic group order as $\mathcal{N} = 2\mathfrak{N}$.

The energy dispersion relations (i.e., electronic band diagrams) can be obtained [\[104\]](#) by first writing the TB Hamiltonian of the flat sheet, and then applying the periodic boundary condition along the direction of chiral vector, \mathbf{C}_h , i.e., $\psi(\mathbf{x} + \mathbf{C}_h) = \psi(\mathbf{x})$. This

leads to the condition $\exp(i\mathbf{k} \cdot \mathbf{C}_h) = 1$ and quantizes the wave vector \mathbf{k}_\perp , thus giving rise to \mathcal{N} discrete wavevectors parallel to \mathbf{k}_\perp , in the direction of \mathbf{C}_h . The wavevector \mathbf{k}_\parallel , which is parallel to the axis of the nanotube, remains continuous, however. Since the two-dimensional sheet is being rolled-up to form a quasi-one-dimensional nanotube, the Brillouin zone (BZ) is one-dimensional, and the condition $\mathbf{T} \cdot \mathbf{k}_\parallel = 2\pi$ implies that the length of the Brillouin zone is $2\pi/T$. Thus, the \mathcal{N} one-dimensional energy dispersion relations for the nanotube can be parametrized as $\epsilon\left(s\mathbf{k}_\perp + \frac{\mathbf{k}_\parallel}{|\mathbf{k}_\parallel|}k\right)$, with $s = 0, \dots, \mathcal{N} - 1$ and $-\frac{\pi}{T} \leq k < \frac{\pi}{T}$.

Note that this construction immediately implies that a zigzag or armchair CKNT of cyclic group order \mathfrak{N} will feature $2\mathfrak{N}$ flat bands, since the starting point is the Kagome graphene TB Hamiltonian (Appendix A.1) featuring a single flat band across its Brillouin zone. This is consistent with the observations made from first principles calculations (Section 3.3).

—

Acknowledgements

This work was supported by grant DE-SC0023432 funded by the U.S. Department of Energy, Office of Science. This research used resources of the National Energy Research Scientific Computing Center, a DOE Office of Science User Facility supported by the Office of Science of the U.S. Department of Energy under Contract No. DE-AC02-05CH11231, using NERSC awards BES-ERCAP0025205 and BES-ERCAP0025168. ASB acknowledges startup support from the Samueli School Of Engineering at UCLA, as well as funding from UCLA's Council on Research (COR) Faculty Research Grant. ASB also acknowledges support through a Faculty Career Development Award from UCLA's Office of Equity, Diversity and Inclusion. ASB would like to thank Felipe Jornada (Stanford Univ.), Giulia Galli (Univ. of Chicago), Garnet Chan (Caltech), Ellad Tadmor (Univ. of Minnesota), Lin Lin (Univ. of California, Berkeley), David J. Singh (Univ. of Missouri), Suneel Kodambaka (Virginia Tech.), Yves Rubin (UCLA) and Rahul Roy (UCLA) for insightful discussions and suggestions, and Neha Bairoliya (Univ. of Southern California) for providing encouragement and support, during the preparation of this manuscript. SS would like to thank Richard D. James (Univ. of Minnesota), and acknowledge financial support from MURI project grant (FA9550-18-1-0095). The authors would like to thank UCLA's Institute for Digital Research and Education (IDRE) and the Minnesota Supercomputing Institute (MSI) for making available some of the computing resources used in this work.

References

- [1] K. Novoselov, D. Jiang, F. Schedin, T. Booth, V. Khotkevich, S. Morozov, A. Geim, Two dimensional atomic crystals, *Proceedings of the National Academy of Sciences* 102 (30) (2005) 10451–10453.
- [2] K. Novoselov, A. Morozov, et. al., [Two-dimensional gas of massless dirac fermions in graphene](https://doi.org/10.1038/nature04233), *Nature* 438 (7065) (2005) 197–200.
URL <https://doi.org/10.1038/nature04233>
- [3] L. Balents, C. R. Dean, D. K. Efetov, A. F. Young, Superconductivity and strong correlations in moiré flat bands, *Nature Physics* 16 (7) (2020) 725–733.
- [4] J.-X. Yin, S. S. Zhang, G. Chang, Q. Wang, S. S. Tsirkin, Z. Guguchia, B. Lian, H. Zhou, K. Jiang, I. Belopolski, et al., Negative flat band magnetism in a spin-orbit-coupled correlated kagome magnet, *Nature Physics* 15 (5) (2019) 443–448.
- [5] O. Derzhko, J. Richter, M. Maksymenko, Strongly correlated flat-band systems: The route from heisenberg spins to hubbard electrons, *International Journal of Modern Physics B* 29 (12) (2015) 1530007.
- [6] C. Elias, G. Fugallo, P. Valvin, C. L’Henoret, J. Li, J. Edgar, F. Sottile, M. Lazzeri, A. Ouerghi, B. Gil, et al., Flat bands and giant light-matter interaction in hexagonal boron nitride, *Physical Review Letters* 127 (13) (2021) 137401.
- [7] V. Iglovikov, F. Hébert, B. Grémaud, G. Batrouni, R. Scalettar, Superconducting transitions in flat-band systems, *Physical Review B* 90 (9) (2014) 094506.
- [8] R. Pons, A. Mielke, T. Stauber, Flat-band ferromagnetism in twisted bilayer graphene, *Physical Review B* 102 (23) (2020) 235101.
- [9] C. Wu, D. Bergman, L. Balents, S. D. Sarma, Flat bands and wigner crystallization in the honeycomb optical lattice, *Physical Review Letters* 99 (7) (2007) 070401.
- [10] M. Shayegan, Wigner crystals in flat band 2d electron systems, *Nature Reviews Physics* 4 (4) (2022) 212–213.
- [11] Y.-F. Wang, H. Yao, C.-D. Gong, D. Sheng, Fractional quantum hall effect in topological flat bands with chern number two, *Physical Review B* 86 (20) (2012) 201101.
- [12] E. Tang, J.-W. Mei, X.-G. Wen, High-temperature fractional quantum hall states, *Physical review letters* 106 (23) (2011) 236802.
- [13] K. Sun, Z. Gu, H. Katsura, S. D. Sarma, Nearly flatbands with nontrivial topology, *Physical review letters* 106 (23) (2011) 236803.
- [14] T. Neupert, L. Santos, C. Chamon, C. Mudry, Fractional quantum hall states at zero magnetic field, *Physical review letters* 106 (23) (2011) 236804.
- [15] E. Y. Andrei, D. K. Efetov, P. Jarillo-Herrero, A. H. MacDonald, K. F. Mak, T. Senthil, E. Tutuc, A. Yazdani, A. F. Young, The marvels of moiré materials, *Nature Reviews Materials* 6 (3) (2021) 201–206.
- [16] L. Wang, E.-M. Shih, A. Ghiotto, L. Xian, D. A. Rhodes, C. Tan, M. Claassen, D. M. Kennes, Y. Bai, B. Kim, et al., Correlated electronic phases in twisted bilayer transition metal dichalcogenides, *Nature materials* 19 (8) (2020) 861–866.
- [17] Y. Cao, V. Fatemi, S. Fang, K. Watanabe, T. Taniguchi, E. Kaxiras, P. Jarillo-Herrero, Unconventional superconductivity in magic-angle graphene superlattices, *Nature* 556 (7699) (2018) 43–50.
- [18] Y. Choi, H. Kim, Y. Peng, A. Thomson, C. Lewandowski, R. Polski, Y. Zhang, H. S. Arora, K. Watanabe, T. Taniguchi, et al., Correlation-driven topological phases in magic-angle twisted bilayer graphene, *Nature* 589 (7843) (2021) 536–541.

- [19] Y. Cao, V. Fatemi, A. Demir, S. Fang, S. L. Tomarken, J. Y. Luo, J. D. Sanchez-Yamagishi, K. Watanabe, T. Taniguchi, E. Kaxiras, et al., Correlated insulator behaviour at half-filling in magic-angle graphene superlattices, *Nature* 556 (7699) (2018) 80–84.
- [20] D. Leykam, A. Andreanov, S. Flach, [Artificial flat band systems: from lattice models to experiments](#), *Advances in Physics: X* 3 (1) (2018) 1473052. doi:10.1080/23746149.2018.1473052. URL <http://dx.doi.org/10.1080/23746149.2018.1473052>
- [21] M. N. Huda, S. Kezilebieke, P. Liljeroth, [Designer flat bands in quasi-one-dimensional atomic lattices](#), *Physical Review Research* 2 (4) (2020) 043426. doi:10.1103/physrevresearch.2.043426. URL <http://dx.doi.org/10.1103/PhysRevResearch.2.043426>
- [22] X. Li, Q. Li, T. Ji, R. Yan, W. Fan, B. Miao, L. Sun, G. Chen, W. Zhang, H. Ding, Lieb lattices formed by real atoms on ag (111) and their lattice constant-dependent electronic properties, *Chinese Physics Letters* 39 (5) (2022) 057301.
- [23] C. Barreateau, F. Ducastelle, T. Mallah, [A bird’s eye view on the flat and conic band world of the honeycomb and kagome lattices: towards an understanding of 2d metal-organic frameworks electronic structure](#), *Journal of Physics: Condensed Matter* 29 (46) (2017) 465302. doi:10.1088/1361-648x/aa8fec. URL <https://doi.org/10.1088/1361-648x/aa8fec>
- [24] G. Tarnopolsky, A. J. Kruchkov, A. Vishwanath, Origin of magic angles in twisted bilayer graphene, *Physical review letters* 122 (10) (2019) 106405.
- [25] C. Naud, G. Faini, D. Maily, Aharonov-bohm cages in 2d normal metal networks, *Physical Review Letters* 86 (22) (2001) 5104.
- [26] J. Vidal, R. Mosseri, B. Douçot, Aharonov-bohm cages in two-dimensional structures, *Physical review letters* 81 (26) (1998) 5888.
- [27] B. R. Ortiz, L. C. Gomes, J. R. Morey, M. Winiarski, M. Bordelon, J. S. Mangum, I. W. Oswald, J. A. Rodriguez-Rivera, J. R. Neilson, S. D. Wilson, et al., New kagome prototype materials: discovery of kv 3 sb 5, rbv 3 sb 5, and csv 3 sb 5, *Physical Review Materials* 3 (9) (2019) 094407.
- [28] M. Li, Q. Wang, G. Wang, Z. Yuan, W. Song, R. Lou, Z. Liu, Y. Huang, Z. Liu, H. Lei, et al., Dirac cone, flat band and saddle point in kagome magnet ymn6sn6, *Nature communications* 12 (1) (2021) 1–8.
- [29] M. Kang, L. Ye, S. Fang, J.-S. You, A. Levitan, M. Han, J. I. Facio, C. Jozwiak, A. Bostwick, E. Rotenberg, et al., Dirac fermions and flat bands in the ideal kagome metal fesn, *Nature materials* 19 (2) (2020) 163–169.
- [30] E. Liu, Y. Sun, N. Kumar, L. Muechler, A. Sun, L. Jiao, S.-Y. Yang, D. Liu, A. Liang, Q. Xu, et al., Giant anomalous hall effect in a ferromagnetic kagome-lattice semimetal, *Nature physics* 14 (11) (2018) 1125–1131.
- [31] D. Liu, A. Liang, E. Liu, Q. Xu, Y. Li, C. Chen, D. Pei, W. Shi, S. Mo, P. Dudin, et al., Magnetic weyl semimetal phase in a kagomé crystal, *Science* 365 (6459) (2019) 1282–1285.
- [32] T. Neupert, M. M. Denner, J.-X. Yin, R. Thomale, M. Z. Hasan, Charge order and superconductivity in kagome materials, *Nature Physics* 18 (2) (2022) 137–143.
- [33] Y.-X. Jiang, J.-X. Yin, M. M. Denner, N. Shumiya, B. R. Ortiz, G. Xu, Z. Guguchia, J. He, M. S. Hossain, X. Liu, et al., Unconventional chiral charge order in kagome superconductor kv3sb5, *Nature Materials* 20 (10) (2021) 1353–1357.
- [34] T.-H. Han, M. Norman, J.-J. Wen, J. A. Rodriguez-Rivera, J. S. Helton, C. Broholm, Y. S. Lee, Correlated impurities and intrinsic spin-liquid physics in the kagome material herbertsmithite, *Physical Review B* 94 (6) (2016) 060409.
- [35] H. Liu, S. Meng, F. Liu, Screening two-dimensional materials with topological flat bands, *Physical*

- Review Materials 5 (8) (2021) 084203.
- [36] C. Zhong, Y. Xie, Y. Chen, S. Zhang, [Coexistence of flat bands and dirac bands in a carbon-kagome-lattice family](#), Carbon 99 (2016) 65–70. doi:<https://doi.org/10.1016/j.carbon.2015.11.073>. URL <https://www.sciencedirect.com/science/article/pii/S0008622315304814>
- [37] C. Zhong, Y. Xie, Y. Chen, S. Zhang, Coexistence of flat bands and dirac bands in a carbon-kagome-lattice family, Carbon 99 (2016) 65–70.
- [38] O. Leenaerts, B. Schoeters, B. Partoens, [Stable kagome lattices from group IV elements](#), Phys. Rev. B 91 (2015) 115202. doi:[10.1103/PhysRevB.91.115202](https://doi.org/10.1103/PhysRevB.91.115202). URL <https://link.aps.org/doi/10.1103/PhysRevB.91.115202>
- [39] B. Sarikavak-Lisesivdin, S. B. Lisesivdin, E. Ozbay, F. Jelezko, [Structural parameters and electronic properties of 2d carbon allotrope: Graphene with a kagome lattice structure](#), Chemical physics letters 760 (2020) 138006–138006. doi:[10.1016/j.cplett.2020.138006](https://doi.org/10.1016/j.cplett.2020.138006). URL <https://doi.org/10.1016/j.cplett.2020.138006>
- [40] Y. Chen, Y. Y. Sun, H. Wang, D. West, Y. Xie, J. Zhong, V. Meunier, M. L. Cohen, S. B. Zhang, [Carbon kagome lattice and orbital-frustration-induced metal-insulator transition for optoelectronics](#), Phys. Rev. Lett. 113 (2014) 085501. doi:[10.1103/PhysRevLett.113.085501](https://doi.org/10.1103/PhysRevLett.113.085501). URL <https://link.aps.org/doi/10.1103/PhysRevLett.113.085501>
- [41] Y. Chen, S. Xu, Y. Xie, C. Zhong, C. Wu, S. B. Zhang, Ferromagnetism and wigner crystallization in kagome graphene and related structures, Phys. Rev. B 98 (2018) 035135. doi:[10.1103/PhysRevB.98.035135](https://doi.org/10.1103/PhysRevB.98.035135).
- [42] D. M. Kennes, L. Xian, M. Claassen, A. Rubio, One-dimensional flat bands in twisted bilayer germanium selenide, Nature communications 11 (1) (2020) 1–8.
- [43] Y. Li, Q. Yuan, D. Guo, C. Lou, X. Cui, G. Mei, H. Petek, L. Cao, W. Ji, M. Feng, One-dimensional electronic flat bands in untwisted moiré superlattices, Advanced Materials (2023) 2300572.
- [44] G. R. Schleder, M. Pizzochero, E. Kaxiras, One-dimensional moiré physics and chemistry in heterostrained bilayer graphene, arXiv preprint arXiv:2306.09799 (2023).
- [45] P. C. Hohenberg, [Existence of long-range order in one and two dimensions](#), Phys. Rev. 158 (1967) 383–386. doi:[10.1103/PhysRev.158.383](https://doi.org/10.1103/PhysRev.158.383). URL <https://link.aps.org/doi/10.1103/PhysRev.158.383>
- [46] N. D. Mermin, H. Wagner, Absence of ferromagnetism or antiferromagnetism in one-or two-dimensional isotropic heisenberg models, Physical Review Letters 17 (22) (1966) 1133.
- [47] K. Arutyunov, D. Golubev, A. Zaikin, [Superconductivity in one dimension](#), Physics Reports 464 (1-2) (2008) 1–70. doi:[10.1016/j.physrep.2008.04.009](https://doi.org/10.1016/j.physrep.2008.04.009). URL <https://doi.org/10.1016%2Fj.physrep.2008.04.009>
- [48] R. Martin, L. Reining, D. Ceperly, Interacting Electrons: Theory and Computational Approaches, Cambridge University Press, 2016.
- [49] R. D. James, Objective structures, Journal of the Mechanics and Physics of Solids 54 (11) (2006) 2354–2390.
- [50] J. M. Kim, M. F. Haque, E. Y. Hsieh, S. M. Nahid, I. Zarin, K.-Y. Jeong, J.-P. So, H.-G. Park, S. Nam, Strain engineering of low-dimensional materials for emerging quantum phenomena and functionalities, Advanced Materials (2022) 2107362.
- [51] C. D. Aiello, M. Abbas, J. Abendroth, A. S. Banerjee, D. Beratan, J. Belling, B. Berche, A. Botana, J. R. Caram, L. Celardo, et al., A chirality-based quantum leap: A forward-looking review, arXiv preprint arXiv:2009.00136 (2020) 4989–5035.
- [52] R. Naaman, D. H. Waldeck, Spintronics and chirality: Spin selectivity in electron transport through chiral molecules, Annual review of physical chemistry 66 (2015) 263–281.

- [53] R. Nakajima, D. Hirobe, G. Kawaguchi, Y. Nabei, T. Sato, T. Narushima, H. Okamoto, H. Yamamoto, Giant spin polarization and a pair of antiparallel spins in a chiral superconductor, *Nature* 613 (7944) (2023) 479–484.
- [54] J. Linder, J. W. Robinson, Superconducting spintronics, *Nature Physics* 11 (4) (2015) 307–315.
- [55] A. Sidorenko, *Functional nanostructures and metamaterials for superconducting spintronics*, Cham, Switzerland: Springer International Publishing (2018).
- [56] F. Qin, W. Shi, T. Ideue, M. Yoshida, A. Zak, R. Tenne, T. Kikitsu, D. Inoue, D. Hashizume, Y. Iwasa, Superconductivity in a chiral nanotube, *Nature communications* 8 (1) (2017) 1–6.
- [57] A. Hirsch, The era of carbon allotropes, *Nature materials* 9 (11) (2010) 868–871.
- [58] R.-S. Zhang, J.-W. Jiang, The art of designing carbon allotropes, *Frontiers of Physics* 14 (1) (2019) 1–17.
- [59] R. Hoffmann, A. A. Kabanov, A. A. Golov, D. M. Proserpio, Homo citans and carbon allotropes: For an ethics of citation, *Angewandte Chemie International Edition* 55 (37) (2016) 10962–10976.
- [60] Z. Li, Y. Xie, Y. Chen, Three-dimensional kagome graphene networks and their topological properties, *Computational Materials Science* 173 (2020) 109406.
- [61] Z. Wang, X.-F. Zhou, X. Zhang, Q. Zhu, H. Dong, M. Zhao, A. R. Oganov, Phagraphene: a low-energy graphene allotrope composed of 5–6–7 carbon rings with distorted dirac cones, *Nano letters* 15 (9) (2015) 6182–6186.
- [62] Y. Chen, Y. Xie, X. Yan, M. L. Cohen, S. Zhang, Topological carbon materials: A new perspective, *Physics Reports* 868 (2020) 1–32.
- [63] P. Yan, T. Ouyang, C. He, J. Li, C. Zhang, C. Tang, J. Zhong, Newly discovered graphyne allotrope with rare and robust dirac node loop, *Nanoscale* 13 (6) (2021) 3564–3571.
- [64] J.-Y. You, B. Gu, G. Su, Flat band and hole-induced ferromagnetism in a novel carbon monolayer, *Scientific Reports* 9 (1) (2019) 1–7. doi:<https://doi.org/10.1038/s41598-019-56738-8>.
- [65] X. Shi, S. Li, J. Li, T. Ouyang, C. Zhang, C. Tang, C. He, J. Zhong, High-throughput screening of two-dimensional planar sp² carbon space associated with a labeled quotient graph, *The Journal of Physical Chemistry Letters* 12 (47) (2021) 11511–11519.
- [66] M. Zhou, Z. Liu, W. Ming, Z. Wang, F. Liu, s d 2 graphene: Kagome band in a hexagonal lattice, *Physical review letters* 113 (23) (2014) 236802.
- [67] M. Maruyama, S. Okada, Interplay between the kagome flat band and the dirac cone in porous graphitic networks, *Carbon* 125 (2017) 530–535.
- [68] M. Endo, S. Iijima, M. S. Dresselhaus, *Carbon nanotubes*, Elsevier, 2013.
- [69] S. Iijima, T. Ichihashi, Single-shell carbon nanotubes of 1-nm diameter, *nature* 363 (6430) (1993) 603.
- [70] K. Wakabayashi, M. Fujita, H. Ajiki, M. Sigrist, Electronic and magnetic properties of nanographite ribbons, *Physical Review B* 59 (12) (1999) 8271.
- [71] Y.-W. Son, M. L. Cohen, S. G. Louie, Energy gaps in graphene nanoribbons, *Physical review letters* 97 (21) (2006) 216803.
- [72] S. Yu, W. Zheng, Q. Wen, Q. Jiang, First principle calculations of the electronic properties of nitrogen-doped carbon nanoribbons with zigzag edges, *Carbon* 46 (3) (2008) 537–543.
- [73] J. Zhang, R. Wang, X. Zhu, A. Pan, C. Han, X. Li, D. Zhao, C. Ma, W. Wang, H. Su, C. Niu, [Pseudo-topotactic conversion of carbon nanotubes to t-carbon nanowires under picosecond laser irradiation in methanol](https://doi.org/10.1038/s41467-017-00817-9), *Nature Communications* 8 (1) (2017) 683. doi:10.1038/s41467-017-00817-9
URL <https://doi.org/10.1038/s41467-017-00817-9>
- [74] V. R. Coluci, S. F. Braga, S. B. Legoas, D. S. Galvão, R. H. Baughman, [Families of carbon](#)

- nanotubes: Graphyne-based nanotubes, *Phys. Rev. B* 68 (2003) 035430. doi:10.1103/PhysRevB.68.035430.
 URL <https://link.aps.org/doi/10.1103/PhysRevB.68.035430>
- [75] V. Coluci, S. Braga, S. Legoas, D. Galvao, R. Baughman, New families of carbon nanotubes based on graphyne motifs, *Nanotechnology* 15 (4) (2004) S142.
- [76] B. Kang, J. Y. Lee, **Electronic properties of alpha-graphyne nanotubes**, *Carbon* 84 (2015) 246–253. doi:<https://doi.org/10.1016/j.carbon.2014.12.002>.
 URL <https://www.sciencedirect.com/science/article/pii/S000862231401152X>
- [77] V. Coluci, D. Galvao, R. Baughman, Theoretical investigation of electromechanical effects for graphyne carbon nanotubes, *The Journal of chemical physics* 121 (7) (2004) 3228–3237.
- [78] B. Kang, J. H. Moon, J. Y. Lee, **Size dependent electronic band structures of beta- and gamma-graphyne nanotubes**, *RSC Adv.* 5 (2015) 80118–80121. doi:10.1039/C5RA12188D.
 URL <http://dx.doi.org/10.1039/C5RA12188D>
- [79] D.-C. Yang, R. Jia, Y. Wang, C.-P. Kong, J. Wang, Y. Ma, R. I. Eglitis, H.-X. Zhang, Novel carbon nanotubes rolled from 6, 6, 12-graphyne: Double dirac points in 1d material, *The Journal of Physical Chemistry C* 121 (27) (2017) 14835–14844.
- [80] K. Wakabayashi, Y. Takane, M. Yamamoto, M. Sigrist, Electronic transport properties of graphene nanoribbons, *New Journal of Physics* 11 (9) (2009) 095016.
- [81] X. Yang, G. Wu, Itinerant flat-band magnetism in hydrogenated carbon nanotubes, *ACS nano* 3 (7) (2009) 1646–1650.
- [82] O. Arroyo-Gascón, R. Fernández-Perea, E. Suárez Morell, C. Cabrillo, L. Chico, **One-dimensional moiré superlattices and flat bands in collapsed chiral carbon nanotubes**, *Nano Letters* 20 (10) (2020) 7588–7593, pMID: 32870695. arXiv:<https://doi.org/10.1021/acs.nanolett.0c03091>, doi:10.1021/acs.nanolett.0c03091.
 URL <https://doi.org/10.1021/acs.nanolett.0c03091>
- [83] O. Arroyo-Gascón, R. Fernández-Perea, E. S. Morell, C. Cabrillo, L. Chico, Universality of moiré physics in collapsed chiral carbon nanotubes, *Carbon* 205 (2023) 394–401.
- [84] M. Koshino, P. Moon, Y.-W. Son, Incommensurate double-walled carbon nanotubes as one-dimensional moiré crystals, *Physical Review B* 91 (3) (2015) 035405.
- [85] Z. Liu, F. Liu, Y.-S. Wu, **Exotic electronic states in the world of flat bands: From theory to material**, *Chinese Physics B* 23 (7) (2014) 077308. doi:10.1088/1674-1056/23/7/077308.
 URL <https://doi.org/10.1088/1674-1056/23/7/077308>
- [86] T. Wavrunek, Q. Peng, N. Abu-Zahra, Mechanical properties and buckling of kagome graphene under tension: A molecular dynamics study, *Crystals* 12 (2) (2022) 292.
- [87] A. Rüegg, J. Wen, G. A. Fiete, Topological insulators on the decorated honeycomb lattice, *Physical Review B* 81 (20) (2010) 205115.
- [88] M. F. López, J. Merino, Magnetism and topological phases in an interacting decorated honeycomb lattice with spin-orbit coupling, *Physical Review B* 102 (3) (2020) 035157.
- [89] M. F. López, B. J. Powell, J. Merino, Topological superconductivity from doping a triplet quantum spin liquid in a flat-band system, *Physical Review B* 106 (23) (2022) 235129.
- [90] J. Merino, M. F. López, B. J. Powell, Unconventional superconductivity near a flat band in organic and organometallic materials, *Physical Review B* 103 (9) (2021) 094517.
- [91] M. Chen, H.-Y. Hui, S. Tewari, V. Scarola, Quantum anomalous hall state from spatially decaying interactions on the decorated honeycomb lattice, *Physical Review B* 97 (3) (2018) 035114.
- [92] J.-W. Rhim, K. Kim, B.-J. Yang, Quantum distance and anomalous landau levels of flat bands, *Nature* 584 (7819) (2020) 59–63.

- [93] R. Pawlak, X. Liu, S. Ninova, P. D’astolfo, C. Drechsel, J.-C. Liu, R. Häner, S. Decurtins, U. Aschauer, S.-X. Liu, et al., On-surface synthesis of nitrogen-doped kagome graphene, *Angewandte Chemie* 133 (15) (2021) 8451–8456.
- [94] X. Li, D. Han, T. Qin, J. Xiong, J. Huang, T. Wang, H. Ding, J. Hu, Q. Xu, J. Zhu, Selective synthesis of kagome nanoporous graphene on ag (111) via an organometallic template, *Nanoscale* 14 (16) (2022) 6239–6247.
- [95] A. Korde, B. Min, E. Kapaca, O. Knio, I. Nezam, Z. Wang, J. Leisen, X. Yin, X. Zhang, D. S. Sholl, et al., Single-walled zeolitic nanotubes, *Science* 375 (6576) (2022) 62–66.
- [96] Y. Wang, K. Wan, F. Pan, X. Zhu, Y. Jiang, H. Wang, Y. Chen, X. Shi, M. Liu, Bamboo-like π -nanotubes with tunable helicity and circularly polarized luminescence, *Angewandte Chemie* 133 (30) (2021) 16751–16757.
- [97] A. S. Banerjee, Density functional methods for Objective Structures: Theory and simulation schemes, Ph.D. thesis, University of Minnesota, Minneapolis (2013).
- [98] A. S. Banerjee, Ab initio framework for systems with helical symmetry: theory, numerical implementation and applications to torsional deformations in nanostructures, *Journal of the Mechanics and Physics of Solids* (2021) 104515.
- [99] H. M. Yu, A. S. Banerjee, Density functional theory method for twisted geometries with application to torsional deformations in group-iv nanotubes, *Journal of Computational Physics* 456 (2022) 111023.
- [100] S. Ghosh, A. S. Banerjee, P. Suryanarayana, Symmetry-adapted real-space density functional theory for cylindrical geometries: Application to large group-IV nanotubes, *Physical Review B* 100 (12) (2019) 125143.
- [101] A. S. Banerjee, P. Suryanarayana, Cyclic density functional theory: A route to the first principles simulation of bending in nanostructures, *Journal of the Mechanics and Physics of Solids* 96 (2016) 605–631.
- [102] S. Pathrudkar, H. M. Yu, S. Ghosh, A. S. Banerjee, Machine learning based prediction of the electronic structure of quasi-one-dimensional materials under strain, *Physical Review B* 105 (2022) 195141. [doi:10.1103/PhysRevB.105.195141](https://doi.org/10.1103/PhysRevB.105.195141).
- [103] S. Agarwal, A. S. Banerjee, Solution of the schrodinger equation for quasi-one-dimensional materials using helical waves, arXiv preprint arXiv:2210.12252 (2022).
- [104] G. Dresselhaus, M. S. Dresselhaus, S. Riichiro, *Physical Properties of Carbon Nanotubes*, World Scientific, 1998.
- [105] T. Dumitrica, R. D. James, Objective molecular dynamics, *Journal of the Mechanics and Physics of Solids* 55 (10) (2007) 2206 – 2236.
- [106] X. Gonze, J.-M. Beuken, R. Caracas, F. Detraux, M. Fuchs, G.-M. Rignanese, L. Sindic, M. Verstraete, G. Zerah, F. Jollet, M. Torrent, A. Roy, M. Mikami, P. Ghosez, J.-Y. Raty, D. Allan, First-principles computation of material properties: the ABINIT software project, *Computational Materials Science* 25 (3) (2002) 478 – 492.
- [107] A. H. Romero, D. C. Allan, B. Amadon, G. Antonius, T. Applencourt, L. Baguet, J. Bieder, F. Bottin, J. Bouchet, E. Bousquet, et al., Abinit: Overview and focus on selected capabilities, *The Journal of chemical physics* 152 (12) (2020) 124102.
- [108] X. Gonze, F. Jollet, F. A. Araujo, D. Adams, B. Amadon, T. Applencourt, C. Audouze, J.-M. Beuken, J. Bieder, A. Bokhanchuk, et al., Recent developments in the abinit software package, *Computer Physics Communications* 205 (2016) 106–131.
- [109] N. Troullier, J. L. Martins, Efficient pseudopotentials for plane-wave calculations, *Physical Review B* 43 (3) (1991) 1993.

- [110] J. P. Perdew, Y. Wang, Accurate and simple analytic representation of the electron-gas correlation energy, *Physical Review B* 45 (1992) 13244–13249.
- [111] J. P. Perdew, K. Burke, M. Ernzerhof, Generalized gradient approximation made simple, *Physical review letters* 77 (18) (1996) 3865.
- [112] A. Van de Walle, G. Ceder, Correcting overbinding in local-density-approximation calculations, *Physical Review B* 59 (23) (1999) 14992.
- [113] N. Hamada, S.-i. Sawada, A. Oshiyama, *New one-dimensional conductors: Graphitic microtubules*, *Phys. Rev. Lett.* 68 (1992) 1579–1581. doi:10.1103/PhysRevLett.68.1579
URL <https://link.aps.org/doi/10.1103/PhysRevLett.68.1579>
- [114] S. B. Sinnott, R. Andrews, *Carbon nanotubes: Synthesis, properties, and applications*, *Critical Reviews in Solid State and Materials Sciences* 26 (3) (2001) 145–249. arXiv:<https://doi.org/10.1080/20014091104189>, doi:10.1080/20014091104189.
URL <https://doi.org/10.1080/20014091104189>
- [115] S. Roy, V. Jain, R. Bajpai, P. Ghosh, A. Pente, B. Singh, D. Misra, Formation of carbon nanotube bucky paper and feasibility study for filtration at the nano and molecular scale, *The Journal of Physical Chemistry C* 116 (35) (2012) 19025–19031.
- [116] B. Corry, Designing carbon nanotube membranes for efficient water desalination, *The Journal of Physical Chemistry B* 112 (5) (2008) 1427–1434.
- [117] E. Frackowiak, F. Beguin, Electrochemical storage of energy in carbon nanotubes and nanostructured carbons, *Carbon* 40 (10) (2002) 1775–1787.
- [118] E. Frackowiak, S. Gautier, H. Gaucher, S. Bonnamy, F. Beguin, Electrochemical storage of lithium in multiwalled carbon nanotubes, *Carbon* 37 (1) (1999) 61–69.
- [119] C. Nützenadel, A. Züttel, D. Chartouni, L. Schlapbach, Electrochemical storage of hydrogen in nanotube materials, *Electrochemical and solid-state letters* 2 (1) (1998) 30.
- [120] P. Giannozzi, S. Baroni, N. Bonini, M. Calandra, R. Car, C. Cavazzoni, D. Ceresoli, G. L. Chiarotti, M. Cococcioni, I. Dabo, A. D. Corso, S. de Gironcoli, S. Fabris, G. Fratesi, R. Gebauer, U. Gerstmann, C. Gougoussis, A. Kokalj, M. Lazzeri, L. Martin-Samos, N. Marzari, F. Mauri, R. Mazzarello, S. Paolini, A. Pasquarello, L. Paulatto, C. Sbraccia, S. Scandolo, G. Sclauzero, A. P. Seitsonen, A. Smogunov, P. Umari, R. M. Wentzcovitch, QUANTUM ESPRESSO: a modular and open-source software project for quantum simulations of materials, *Journal of Physics: Condensed Matter* 21 (39) (2009) 395502.
- [121] P. Giannozzi, O. Andreussi, T. Brumme, O. Bunau, M. B. Nardelli, M. Calandra, R. Car, C. Cavazzoni, D. Ceresoli, M. Cococcioni, et al., Advanced capabilities for materials modelling with quantum espresso, *Journal of physics: Condensed matter* 29 (46) (2017) 465901.
- [122] P. Giannozzi, O. Baseggio, P. Bonfà, D. Brunato, R. Car, I. Carnimeo, C. Cavazzoni, S. De Gironcoli, P. Delugas, F. Ferrari Ruffino, et al., Quantum espresso toward the exascale, *The Journal of chemical physics* 152 (15) (2020) 154105.
- [123] W. Hu, L. Lin, C. Yang, Dgdf: A massively parallel method for large scale density functional theory calculations, *The Journal of chemical physics* 143 (12) (2015) 124110.
- [124] L. Lin, J. Lu, L. Ying, E. Weinan, Adaptive local basis set for kohn–sham density functional theory in a discontinuous galerkin framework i: Total energy calculation, *Journal of Computational Physics* 231 (4) (2012) 2140–2154.
- [125] W. Jia, L.-W. Wang, L. Lin, Parallel transport time-dependent density functional theory calculations with hybrid functional on summit, in: *Proceedings of the International Conference for High Performance Computing, Networking, Storage and Analysis*, 2019, pp. 1–23.
- [126] W. Hu, L. Lin, A. S. Banerjee, E. Vecharynski, C. Yang, Adaptively compressed exchange operator

- for large-scale hybrid density functional calculations with applications to the adsorption of water on silicene, *Journal of chemical theory and computation* 13 (3) (2017) 1188–1198.
- [127] W. Kohn, L. J. Sham, Self-consistent equations including exchange and correlation effects, *Physical Review* 140 (4A) (1965) 1133–1138.
- [128] Y. Hakobyan, E. Tadmor, R. James, Objective quasicontinuum approach for rod problems, *Physical Review B* 86 (24) (2012) 245435.
- [129] E. B. Barros, A. Jorio, G. G. Samsonidze, R. B. Capaz, A. G. S. Filho, J. M. Filho, G. Dresselhaus, M. S. Dresselhaus, Review on the symmetry-related properties of carbon nanotubes, *Physics Reports* 431 (6) (2006) 261 – 302.
- [130] L. Kleinman, D. Bylander, Efficacious form for model pseudopotentials, *Physical Review Letters* 48 (20) (1982) 1425.
- [131] N. Troullier, J. L. Martins, Efficient pseudopotentials for plane-wave calculations, *Physical review B* 43 (3) (1991) 1993.
- [132] E. Bitzek, P. Koskinen, F. Gähler, M. Moseler, P. Gumbsch, Structural relaxation made simple, *Physical Review Letters* 97 (17) (2006) 170201.
- [133] J. P. Perdew, Y. Wang, Accurate and simple analytic representation of the electron-gas correlation energy, *Physical Review B* 45 (23) (1992) 13244.
- [134] J. R. Chelikowsky, N. Troullier, Y. Saad, Finite-difference-pseudopotential method: Electronic structure calculations without a basis, *Physical review letters* 72 (8) (1994) 1240.
- [135] J. R. Chelikowsky, N. Troullier, K. Wu, Y. Saad, Higher order finite difference pseudopotential method: An application to diatomic molecules, *Phys. Rev. B* 50 (1994) 11355–11364.
- [136] X. Jing, N. Troullier, D. Dean, N. Binggeli, J. R. Chelikowsky, K. Wu, Y. Saad, Ab initio molecular-dynamics simulations of si clusters using the higher-order finite-difference-pseudopotential method, *Physical Review B* 50 (16) (1994) 12234–12237.
- [137] H. Kikuchi, O. Tomoya, F. Yoshitaka, T. Shigeru, *First-principles calculations in real-space formalism: electronic configurations and transport properties of nanostructures*, World Scientific, 2005.
- [138] S. Ghosh, P. Suryanarayana, SPARC: Accurate and efficient finite-difference formulation and parallel implementation of density functional theory: Isolated clusters, *Computer Physics Communications* 212 (2017) 189–204.
- [139] S. Ghosh, P. Suryanarayana, SPARC: Accurate and efficient finite-difference formulation and parallel implementation of density functional theory: Extended systems, *Computer Physics Communications* 216 (2017) 109–125.
- [140] D. Marx, J. Hutter, *Ab initio molecular dynamics: basic theory and advanced methods*, 1st Edition, Cambridge University Press, 2009.
- [141] R. M. Martin, *Electronic Structure: Basic Theory and Practical Methods*, 1st Edition, Cambridge University Press, 2004.
- [142] D. Hamann, Optimized norm-conserving vanderbilt pseudopotentials, *Physical Review B* 88 (8) (2013) 085117.
- [143] M. Schlipf, F. Gygi, Optimization algorithm for the generation of oncv pseudopotentials, *Computer Physics Communications* 196 (2015) 36–44.
- [144] D. C. Liu, J. Nocedal, On the limited memory bfgs method for large scale optimization, *Mathematical programming* 45 (1) (1989) 503–528.
- [145] D. J. Evans, B. L. Holian, The nose–hoover thermostat, *The Journal of chemical physics* 83 (8) (1985) 4069–4074.
- [146] G. J. Martyna, M. L. Klein, M. Tuckerman, Nosé–hoover chains: The canonical ensemble via continuous dynamics, *The Journal of chemical physics* 97 (4) (1992) 2635–2643.

- [147] G. Prandini, A. Marrazzo, I. E. Castelli, N. Mounet, N. Marzari, A standard solid state pseudopotentials (SSSP) library optimized for precision and efficiency, materials Cloud Archive 2021.76, <https://doi.org/10.24435/materialscloud:rz-77> (2021).
- [148] G. Prandini, A. Marrazzo, I. E. Castelli, N. Mounet, N. Marzari, Precision and efficiency in solid-state pseudopotential calculations, *npj Computational Materials* 4 (1) (2018) 1–13.
- [149] M. S. Dresselhaus, G. Dresselhaus, P. C. Eklund, *Science of fullerenes and carbon nanotubes: their properties and applications*, Elsevier, 1996.
- [150] M. Dresselhaus, G. Dresselhaus, R. Saito, *Physics of carbon nanotubes*, *Carbon* 33 (7) (1995) 883–891.
- [151] L. V. Liu, W. Q. Tian, Y. A. Wang, Ab initio studies of vacancy-defected fullerenes and single-walled carbon nanotubes, *International Journal of Quantum Chemistry* 109 (14) (2009) 3441–3456.
- [152] H. Shin, S. Kang, J. Koo, H. Lee, J. Kim, Y. Kwon, Cohesion energetics of carbon allotropes: Quantum monte carlo study, *The Journal of chemical physics* 140 (11) (2014) 114702.
- [153] Y. Hu, C. Wu, Q. Pan, Y. Jin, R. Lyu, V. Martinez, S. Huang, J. Wu, L. J. Wayment, N. A. Clark, et al., Synthesis of γ -graphyne using dynamic covalent chemistry, *Nature Synthesis* (2022) 1–6.
- [154] V. G. Desyatkin, W. B. Martin, A. E. Aliev, N. E. Chapman, A. F. Fonseca, D. S. Galvão, E. R. Miller, K. H. Stone, Z. Wang, D. Zakhidov, et al., Scalable synthesis and characterization of multilayer γ -graphyne, new carbon crystals with a small direct band gap, *Journal of the American Chemical Society* (2022) 17999–18008.
- [155] Q. Li, Y. Li, Y. Chen, L. Wu, C. Yang, X. Cui, Synthesis of γ -graphyne by mechanochemistry and its electronic structure, *Carbon* 136 (2018) 248–254.
- [156] H. Zhang, Z. Yao, J. Wang, W. Zhong, Phonon dispersion analysis of carbon nanotubes based on inter-belt model and symplectic solution method, *International Journal of Solids and Structures* 44 (20) (2007) 6428–6449.
- [157] R. Jishi, L. Venkataraman, M. Dresselhaus, G. Dresselhaus, Phonon modes in carbon nanotubes, *Chemical Physics Letters* 209 (1-2) (1993) 77–82.
- [158] R. Saito, T. Takeya, T. Kimura, G. Dresselhaus, M. Dresselhaus, Raman intensity of single-wall carbon nanotubes, *Physical Review B* 57 (7) (1998) 4145.
- [159] J. Kürti, G. Kresse, H. Kuzmany, First-principles calculations of the radial breathing mode of single-wall carbon nanotubes, *Physical Review B* 58 (14) (1998) R8869.
- [160] Z. Yao, C.-C. Zhu, M. Cheng, J. Liu, Mechanical properties of carbon nanotube by molecular dynamics simulation, *Computational Materials Science* 22 (3-4) (2001) 180–184.
- [161] T. Tang, A. Jagota, C.-Y. Hui, N. J. Glassmaker, Collapse of single-walled carbon nanotubes, *Journal of Applied Physics* 97 (7) (2005) 074310.
- [162] J. Xiao, B. Liu, Y. Huang, J. Zuo, K. Hwang, M. Yu, Collapse and stability of single-and multi-wall carbon nanotubes, *Nanotechnology* 18 (39) (2007) 395703.
- [163] J. A. Elliott, J. K. Sandler, A. H. Windle, R. J. Young, M. S. Shaffer, Collapse of single-wall carbon nanotubes is diameter dependent, *Physical Review Letters* 92 (9) (2004) 095501.
- [164] S. Timoshenko, D. H. Young, *Elements of strength of materials*, Van Nostrand Princeton, NJ, 1968.
- [165] J. Ding, X. Yan, J. Cao, Analytical relation of band gaps to both chirality and diameter of single-wall carbon nanotubes, *Physical Review B* 66 (7) (2002) 073401.
- [166] T. T. Heikkilä, N. B. Kopnin, G. E. Volovik, *Flat bands in topological media*, *JETP Letters* 94 (3) (2011) 233–239. doi:10.1134/s0021364011150045. URL <https://doi.org/10.1134/s0021364011150045>
- [167] B. Dóra, I. F. Herbut, R. Moessner, Occurrence of nematic, topological, and berry phases when a

- flat and a parabolic band touch, *Physical Review B* 90 (4) (2014) 045310.
- [168] H.-M. Guo, M. Franz, [Topological insulator on the kagome lattice](#), *Phys. Rev. B* 80 (2009) 113102. doi:10.1103/PhysRevB.80.113102. URL <https://link.aps.org/doi/10.1103/PhysRevB.80.113102>
- [169] E. Tang, J.-W. Mei, X.-G. Wen, [High-temperature fractional quantum hall states](#), *Phys. Rev. Lett.* 106 (2011) 236802. doi:10.1103/PhysRevLett.106.236802. URL <https://link.aps.org/doi/10.1103/PhysRevLett.106.236802>
- [170] D. Yudin, D. Hirschmeier, H. Hafermann, O. Eriksson, A. I. Lichtenstein, M. I. Katsnelson, [Fermi condensation near van hove singularities within the hubbard model on the triangular lattice](#), *Phys. Rev. Lett.* 112 (2014) 070403. doi:10.1103/PhysRevLett.112.070403. URL <https://link.aps.org/doi/10.1103/PhysRevLett.112.070403>
- [171] M. Cutler, N. F. Mott, Observation of anderson localization in an electron gas, *Physical Review* 181 (3) (1969) 1336.
- [172] A. Lagendijk, B. Van Tiggelen, D. S. Wiersma, Fifty years of anderson localization, *Phys. today* 62 (8) (2009) 24–29.
- [173] L. Van Hove, The occurrence of singularities in the elastic frequency distribution of a crystal, *Physical Review* 89 (6) (1953) 1189.
- [174] K. Sun, H. Yao, E. Fradkin, S. A. Kivelson, Topological insulators and nematic phases from spontaneous symmetry breaking in 2d fermi systems with a quadratic band crossing, *Physical Review Letters* 103 (4) (2009) 046811.
- [175] M. Milićević, G. Montambaux, T. Ozawa, O. Jamadi, B. Real, I. Sagnes, A. Lemaître, L. Le Gratiet, A. Harouri, J. Bloch, et al., Type-iii and tilted dirac cones emerging from flat bands in photonic orbital graphene, *Physical Review X* 9 (3) (2019) 031010.
- [176] J.-W. Rhim, B.-J. Yang, Classification of flat bands according to the band-crossing singularity of bloch wave functions, *Physical Review B* 99 (4) (2019) 045107.
- [177] Y. Gomes, R. O. Ramos, Tilted dirac cone effects and chiral symmetry breaking in a planar four-fermion model, *Physical Review B* 104 (24) (2021) 245111.
- [178] R. Naaman, D. H. Waldeck, Chiral-induced spin selectivity effect, *The journal of physical chemistry letters* 3 (16) (2012) 2178–2187.
- [179] J. M. Murray, O. Vafek, Renormalization group study of interaction-driven quantum anomalous hall and quantum spin hall phases in quadratic band crossing systems, *Physical Review B* 89 (20) (2014) 201110.
- [180] S. Uebelacker, C. Honerkamp, Instabilities of quadratic band crossing points, *Physical Review B* 84 (20) (2011) 205122.
- [181] Y. Chong, X.-G. Wen, M. Soljačić, Effective theory of quadratic degeneracies, *Physical Review B* 77 (23) (2008) 235125.
- [182] L. Yang, M. Anantram, J. Han, J. Lu, Band-gap change of carbon nanotubes: Effect of small uniaxial and torsional strain, *Physical Review B* 60 (19) (1999) 13874.
- [183] D. Zhang, R. D. James, T. Dumitrica, Electromechanical characterization of carbon nanotubes in torsion via symmetry adapted tight-binding objective molecular dynamics, *Physical Review B* 80 (11) (2009) 115418.
- [184] L. Yang, J. Han, Electronic structure of deformed carbon nanotubes, *Physical review letters* 85 (1) (2000) 154.
- [185] R. Heyd, A. Charlier, E. McRae, Uniaxial-stress effects on the electronic properties of carbon nanotubes, *Physical Review B* 55 (11) (1997) 6820.
- [186] A. Mayer, Band structure and transport properties of carbon nanotubes using a local pseudopo-

- tential and a transfer-matrix technique, *Carbon* 42 (10) (2004) 2057–2066.
- [187] S. Sharma, A. S. Banerjee, Strain engineering of flat bands in quasi-one-dimensional materials, (in preparation) (2022).
- [188] Y. Chen, Y. Sun, H. Wang, D. West, Y. Xie, J. Zhong, V. Meunier, M. L. Cohen, S. Zhang, Carbon kagome lattice and orbital-frustration-induced metal-insulator transition for optoelectronics, *Physical review letters* 113 (8) (2014) 085501.
- [189] A. Tyagi, R. S. Ningthoujam, *Handbook on Synthesis Strategies for Advanced Materials: Volume-III: Materials Specific Synthesis Strategies*, Springer, 2021.
- [190] G. Qin, K.-R. Hao, Q.-B. Yan, M. Hu, G. Su, Exploring t-carbon for energy applications, *Nanoscale* 11 (13) (2019) 5798–5806.
- [191] T. Guo, P. Nikolaev, A. Thess, D. T. Colbert, R. E. Smalley, Catalytic growth of single-walled nanotubes by laser vaporization, *Chemical physics letters* 243 (1-2) (1995) 49–54.
- [192] M. Kumar, Y. Ando, Chemical vapor deposition of carbon nanotubes: a review on growth mechanism and mass production, *Journal of nanoscience and nanotechnology* 10 (6) (2010) 3739–3758.
- [193] E. Costa Girão, L. Liang, E. Cruz-Silva, A. G. S. Filho, V. Meunier, [Emergence of atypical properties in assembled graphene nanoribbons](#), *Phys. Rev. Lett.* 107 (2011) 135501. doi:10.1103/PhysRevLett.107.135501.
URL <https://link.aps.org/doi/10.1103/PhysRevLett.107.135501>
- [194] P. Han, K. Akagi, F. Federici Canova, R. Shimizu, H. Oguchi, S. Shiraki, P. S. Weiss, N. Asao, T. Hitosugi, Self-assembly strategy for fabricating connected graphene nanoribbons, *ACS nano* 9 (12) (2015) 12035–12044.
- [195] O. G. Schmidt, K. Eberl, Thin solid films roll up into nanotubes, *Nature* 410 (6825) (2001) 168–168.
- [196] A. L. Fetter, J. D. Walecka, *Quantum theory of many-particle systems*, Courier Corporation, 2012.
- [197] S. M. Girvin, K. Yang, *Modern condensed matter physics*, Cambridge University Press, 2019.
- [198] W. Jiang, M. Kang, H. Huang, H. Xu, T. Low, F. Liu, Topological band evolution between lieb and kagome lattices, *Physical Review B* 99 (12) (2019) 125131.
- [199] J.-Y. You, B. Gu, G. Su, Flat band and hole-induced ferromagnetism in a novel carbon monolayer, *Scientific reports* 9 (1) (2019) 1–7.